HHS Public Access

Author manuscript

Exp Eye Res. Author manuscript; available in PMC 2017 November 01.

Published in final edited form as:

Exp Eye Res. 2016 November ; 152: 10–33. doi:10.1016/j.exer.2016.08.020.

Glucocorticoid action in human corneal epithelial cells establishes roles for corticosteroids in wound healing and barrier function of the eye

Mahita Kadmiel[a], **Agnes Janoshazi**[a], **Xiaojiang Xu**[b], and **John A Cidlowski**[a,*]

[a] Signal Transduction Laboratory, National Institute of Environmental Health Sciences, National Institutes of Health, Department of Health and Human Services, Research Triangle Park, North Carolina, USA

[b] Integrative Bioinformatics, National Institute of Environmental Health Sciences, National Institutes of Health, Department of Health and Human Services, Research Triangle Park, North Carolina, USA

Abstract

Glucocorticoids play diverse roles in almost all physiological systems of the body, including both anti-inflammatory and immunosuppressive roles. Synthetic glucocorticoids are one of the most widely prescribed drugs and are used in the treatment of conditions such as autoimmune diseases, allergies, ocular disorders and certain types of cancers. In the interest of investigating glucocorticoid actions in the cornea of the eye, we established that multiple cell types in mouse corneas express functional glucocorticoid receptor (GR) with corneal epithelial cells having robust expression. To define glucocorticoid actions in a cell type-specific manner, we employed immortalized human corneal epithelial (HCE) cell line to define the glucocorticoid transcriptome and elucidated its functions in corneal epithelial cells. Over 4000 genes were significantly regulated within 6 hours of dexamethasone treatment, and genes associated with cell movement, cytoskeletal remodeling and permeability were highly regulated. Real-time *in vitro* wound healing assays revealed that glucocorticoids delay wound healing by attenuating cell migration. These functional alterations were associated with cytoskeletal remodeling at the wounded edge of a scratch-wounded monolayer. However, glucocorticoid treatment improved the organization of tight-junction proteins and enhanced the epithelial barrier function. Our results demonstrate that glucocorticoids profoundly alter corneal epithelial gene expression and many of these changes likely impact both wound healing and epithelial cell barrier function.

* Corresponding author and the person to whom reprints should be addressed: John A. Cidlowski, Ph.D., Chief, Signal Transduction Laboratory and Principal Investigator, National Institute of Environmental Health Sciences, Research Triangle Park, North Carolina., Tel (919) 541-1564, Fax (919) 541-2429, cidlows1@niehs.nih.gov.

Disclosure Statement: The authors have nothing to disclose.

Keywords

Cornea; glucocorticoids; gene expression; wound healing; migration; cytoskeleton; epithelial integrity

1. Introduction

Glucocorticoids are steroid hormones that have a critical role in regulating stress response in the body. Endogenous glucocorticoids in humans are necessary for life and they are synthesized by the adrenal cortex in a tight regulation by the hypothalamic-pituitary-adrenal axis. Both endogenous glucocorticoids and their synthetic derivatives used in patient treatment signal through their canonical receptor, the glucocorticoid receptor (gene name *NR3C1*) that belongs to the super family of nuclear receptors. Glucocorticoid actions span a wide range of cellular and systemic effects including cell cycle, cell movement, glucose homeostasis and fluid regulation. They are most known for their anti-inflammatory and immunosuppressive roles. Due to their potent immunosuppressive property, glucocorticoids have been exploited pharmacologically and they have become one of the largest selling class of drugs in the world today. The nearly ubiquitous expression of the glucocorticoid receptor suggests a role for glucocorticoid signaling in every cell type, which is further supported by studies establishing that glucocorticoid signaling is indeed cell type-specific. For example, glucocorticoids exert an anti-apoptotic role in cardiomyocytes (1) while exerting a pro-apoptotic role in lymphocytes (2). Cell type specificity of glucocorticoid signaling diversifies the actions of glucocorticoids and therefore, there is a need to understand the role of glucocorticoids in a cell/tissue-specific manner.

The cornea is the clear part of the eye that covers the iris, pupil and the anterior chamber. By providing a physical barrier, the cornea protects the interior of the eye from external agents such as bacteria, viruses and debris. By refracting light through the lens and onto the retina where the light signal converts into vision, the cornea also plays an important role in maintaining vision. Synthetic glucocorticoids have been widely used to successfully treat several ocular disorders, however, the functions of glucocorticoid receptor signaling in the eye, particularly in the cornea are largely under studied. Corticosteroids are also used in transplant surgeries such as in lens transplantation and keratoplasty, to minimize graft rejection. Corticosteroids are used in treating sight-threatening conditions of the cornea such as corneal inflammation and corneal neovascularization (3). Despite the fact that glucocorticoids have numerous benefits in treating ocular conditions, some patients receiving chronic glucocorticoid treatment are susceptible to increase in intraocular pressure that could develop into steroid-induced glaucoma and eventually loss of vision (4). Opacification of the lens or cataract formation are also adverse events seen in sustained corticosteroid use. Glucocorticoids have also been reported to be synthesized in the human ocular surface and they have the ability to regulate corneal immune response (5-7). In the cornea, glucocorticoids have been shown to regulate their circadian rhythm (8,9), inhibit blood and lymphatic vessel growth (10,11), curb inflammation (12-15), and increase epithelial integrity under a hypoxic challenge (16), as well as retard wound healing in rabbits (17). Although it has been established that corticosteroids are effective in treating diseases of

the cornea, the molecular functions in specific cell types where they occur have not been fully characterized.

In the current investigation, we establish that mouse corneas express functional GR with strong expression of GR by the corneal epithelial cells. Subsequently, we employed immortalized corneal epithelial cell line derived from human cornea to understand glucocorticoid signaling in a single cell type. Here we demonstrate that glucocorticoids can profoundly alter the gene expression profile of human corneal epithelial cells. Ingenuity pathway analysis (IPA) of the glucocorticoid transcriptome revealed that glucocorticoid signaling in corneal epithelial cells was enriched for genes involved in pathways associated with inflammatory diseases and organismal growth and development. Additionally, Ingenuity Pathway Analysis indicated that glucocorticoid signaling in corneal epithelial cells may regulate cellular functions, such as cell movement and cell growth, by altering the expression of a large cohort of genes. Since cornea is at the interface with the environment and prone to injuries, we focused our further analysis of glucocorticoid signaling in corneal epithelial cells on wound healing which included processes such as cell migration, cytoskeletal remodeling and epithelial permeability. Real time *in vitro* wound healing assays demonstrated that glucocorticoid treatment delayed wound healing of HCE cell monolayer by altering their cytoskeleton. Interestingly, the distribution of tight junction proteins and paracellular permeability in response to glucocorticoid treatment indicated that glucocorticoids enhance barrier function in corneal epithelial cells. The study presented here provides a new understanding of the diversity of glucocorticoid actions on corneal epithelial cell wound healing and barrier function.

2. Materials and methods

2.1 Animals

Wild type C57BL/6 female mice aged 2-months old purchased from Charles River Laboratories were used for all animal experiments. For dexamethasone treatment studies, mice were adrenalectomized at Charles River Laboratories to remove endogenous glucocorticoids and were rested for a week after the surgery before being shipped to the National Institute of Environmental Health Sciences (NIEHS). Upon arrival at NIEHS, the animals were rested for 7-10 days before being treated. For dexamethasone treatment experiment, each mouse was treated with vehicle in the left eye and dexamethasone in the right eye. Dexamethasone was purchased from Steraloids and was prepared in Refresh artificial tears manufactured by Allergan, Irvine, CA. For each animal, one eye received 3 microliters of vehicle (Refresh artificial tears) or dexamethasone prepared at a concentration of 1mg/ml. Six hours after the treatment, mice were euthanized by cervical dislocation and eyes were enucleated and corneas were dissected immediately and stored in RNA later (Qiagen) at 4°C overnight. Six corneas were pooled to generate one sample of RNA, therefore, requiring 24 corneas/treatment to generate an n of 4. RNA was extracted using Trizol and chloroform and purified using RNeasy Micro kit and Dnase digested (Qiagen). For immunofluorescence studies, mice were euthanized by cervical dislocation and eyes were enucleated from euthanized animals. Eyes were fresh frozen in Optimal Cutting Temperature (O.C.T.) Compound (VWR, Pennsylvania) and six-micron sections were

prepared. Sections were stained at 4°C overnight wi th antibodies to glucocorticoid receptor (Cell Signaling, cat#3660, 1:300). Hoechst 33342 and Alexa Fluor 488 Phalloidin (both from Life Technologies, New York) were used to visualize nuclei and actin filaments, respectively. Z-stack images were taken using the Zeiss LSM710 and Zen 2012 software and Image J software were used to process the images.

2.2 Cell culture and treatment

A widely studied immortalized human corneal epithelial cell line (HCE) obtained from RIKEN was used (18). HCE cells were cultured in DMEM/F12 medium supplemented with 5% fetal bovine serum, 5ug/ml insulin, 10ng/ml human epidermal growth factor, 0.5% dimethyl sulfoxide and antibiotics. Anti-glucocorticoid-RU486 (mifepristone) were purchased from Steraloids. Cells were incubated in DMEM/F12 medium containing 5% charcoal stripped fetal bovine serum for 18-24hours before being treated with vehicle or dexamethasone or RU486.

2.3 RNA Isolation and Quantitative RT-PCR Analysis

Total RNA was isolated using the RNeasy Kit (micro kit for Trizol/Chloroform extracted mouse corneal RNA and mini kit for human cells) and DNase digested using the RNase-Free DNase Kit (Qiagen) according to the manufacturer's protocol. The abundance of individual mRNAs was determined using a Taqman one-step RT-PCR method on a 7900HT sequence detection system (Applied Biosystems). Pre-developed Taqman primer probe sets for *GILZ* (Hs00608272_m1, Mm00726417_s1), *FKBP5* (Mm00487406_m1), *TNFRSF11b (Hs00900358_m1)*, BDNF (Hs00380947_m1), EREG (Hs00154995_m1), NGF (Hs00171458_m1) and *PPIB* (Hs00168719_m1, Mm00478295_m1) were purchased from Life Technologies, Grand Island, NY. Target gene expression was normalized to the housekeeping gene *PPIB*, which is not regulated by glucocorticoids.

2.4 SDS-PAGE and Immunoblot Analyses

Cells were washed with ice-cold phosphate buffered saline and lysed in SDS sample buffer (Life Technologies) supplemented with B-mercaptoethanol (final concentration 2.5%). Samples were sonicated on ice for 5 seconds and boiled for 5 mins and 104° centigrade. Equal amounts of protein was loaded and run on precast 10% Tris Mini Protean TGX gels (Bio-Rad) and transferred to nitrocellulose. The membranes were blocked for an hour in LI-COR Blocking buffer at room temperature and then incubated overnight at 4C with primary antibody to GR(19) (1:1000 dilution) or B-actin (Millipore, 1:20,000 dilution). Blots were washed and incubated with goat anti-rabbit IRDye 680-conjugated secondary antibody and/or goat anti-mouse IRDye800-conjugated secondary antibody (Rockland Immunochemicals) for one hour at room temperature. LICOR Odyssey scanner was used to visualize the western blot.

2.5 Microarray and data analysis

Global gene expression analysis was performed on RNA isolated from cells treated with vehicle or Dexamethasone (100nM) for 6 hours (n = 4 biological replicates/treatment). Specifically, gene expression analysis was conducted using Agilent Whole Human Genome

4×44 multiplex format oligo arrays (014850) (Agilent Technologies) following the Agilent 1-color microarray-based gene expression analysis protocol. Starting with 400ng of total RNA, Cy3 labeled cRNA was produced according to manufacturer's protocol. For each sample, 1.65ug of Cy3 labeled cRNAs were fragmented and hybridized for 17 hours in a rotating hybridization oven. Slides were washed and then scanned with an Agilent Scanner. Data was obtained using the Agilent Feature Extraction software (v9.5), using the 1-color defaults for all parameters. The Agilent Feature Extraction Software performed error modeling, adjusting for additive and multiplicative noise.

Differential gene expression was examined using the Partek Genomics Suite V 6.6 (Partek, Inc., St. Louis, MO, USA). To identify differentially expressed probe sets, analysis of variance (ANOVA) was performed and significant changes in gene expression were defined on the basis of p-value ($p < 0.01$). Partek Genomics Suite was further used to generate heat maps for visual analyses and to support generation of hierarchical clustering dendrograms. Lists of significant probe sets were further analyzed using Ingenuity Pathway Analysis (IPA, Content version 27216297) (Ingenuity Systems, Redwood City, CA). Enrichment or overlap was determined by IPA using Fisher's exact test ($p < 0.05$). Pathdesigner feature of IPA was used to build pathways of glucocorticoid-regulated genes. Gene network of genes involved in Cell Movement was extracted from STRING (Version10, http://string-db.org/) and Visualized using Gephi (Version 0.9.1).

2.6 *In vitro* wound healing assay

HCE cells were grown to 90% confluence in 12-well plates in DMEM/F12 medium containing 5% charcoal stripped bovine serum and antibiotics. The cells were then treated with vehicle or dexamethasone or RU486 or both in the same medium containing charcoal stripped fetal bovine serum. After treatment for 24hours, a scratch was made using a sterile 200ul yellow pipette tip in the middle of the confluent monolayer. The wells were washed with the respective treatment media to remove detached and dead cells. The wells were replaced with fresh medium containing the respective treatments. Three to five bright-field images were taken along the scratch area every thirty minutes for up to 30 hours (until the scratch wound is healed) using an incubator setup with a Zeiss LSM 710 confocal microscope using a low-magnification objective of 5X to cover a large area of the healing monolayer. Images were taken only in X and Y planes. Area of wound closure was measured using the following formula:

$$\text{Percent wound closed} = ((\text{Area of wound at 0hr} - \text{area of wound at 18hr}) / \text{area of wound at 0hr} * 100).$$

2.7 Lamellipodia and Filopodia Visualization and Quantification

HCE cells were grown to 90% confluence in glass-bottom dishes and in DMEM/F12 medium containing 5% charcoal stripped bovine serum and antibiotics. The cells were then treated with vehicle or dexamethasone (1000nM) in the same medium containing charcoal stripped medium. After treatment for 24hours, a scratch was made using a sterile 10ul pipette tip in the middle of the confluent monolayer. The wells were replaced with fresh medium containing the respective treatments. The media was discarded and the plates were

washed with the respective treatment media to remove detached and dead cells. To visualize the cell membrane with lamellipodia and filopodia, CellMask™ Deep Red Plasma membrane Stain (Catalog # C10046) was added to the plates at 0.1% concentration in HCE culture medium immediately after creating a scratch wound in the monolayer and imaging at high-magnification (40X oil-immersion objective) was initiated within 10 minutes of making the scratch. Zeiss LSM 780 confocal microscope equipped with an incubator set at 37 degrees centigrade and 5% carbon dioxide was used. Z-stack images scanning a total depth of 6-10 microns (0.75 micron per Z-section) were taken continuously for an hour to visualize the dynamic lamellipodia and filopodia at the healing edge. Maximum intensity projection of a Z-stack of images was made to count the number of filopodia in each image. The number of filopodia on each of the three to five fields (each field had a scratched edge of 250 microns) were manually counted at different time-points starting from 10 minutes to 1 hour after creating a scratch wound and the average number of filopodia were represented.

2.8 Permeability Assays

HCE cells were plated grown to confluence in 12-well transwell plates (Corning Costar Transwell, 0.4uM pore size). Twenty-four hours prior to treatment, the medium was replaced with DMEM/F12 containing 5% charcoal stripped fetal bovine serum. Cells were treated with either vehicle or 100nM dexamethasone for 24 hours. At the end of incubation, FITC Dextran -10kD at a final concentration of 1mg/ml final concentration (purchased from Sigma) was carefully added to the medium in the insert and the plates were returned back to the incubator. After an hour of incubation, media was collected from the bottom wells and the relative units of fluorescence of FITC dextran diffused through the monolayer in the inserts were measured using a fluorescent plate reader.

2.9 Proliferation Assays

For proliferation assays, HCE cells were plated at a density of 8×10^5 cells per well in 6-well cell culture plates. Twenty-four hours after plating, cells were treated with vehicle or dexamethasone (100nM or 1000nM) in DMEM/F12 medium containing charcoal stripped serum. Trypsinized cells and dead floating cells in the supernatant from each well at all time-points (24, 48, and 72 hours post treatment) were counted with Countess Automated Cell Counter (Invitrogen) using chamber slides with a 1:1 dilution of cells to Trypan blue stain 0.4% (Invitrogen). Each sample was counted in duplicate. Average number of viable and dead cells were calculated from 4 independent experiments.

2.10 Flow Cytometric Analysis

Cell proliferation was assessed by flow cytometry. HCE cells were grown in 6-well cell culture plates and treated with vehicle or dexamethasone (100nM or 1000nM) for 24, 48 and 72 hours. After treatment, cells (including floating cells) were collected by trypsinization and propidium iodide was added to identify dead cells. Cells were excited using a 488-nm argon laser and emission was detected at 585 nm. Analysis was carried out using a Becton Dickinson FACSort flow cytometer (Franklin Lakes, NJ, USA) and CELLQuest software (Becton Dickinson Immunocytometry Systems, San Jose, CA, USA).

2.11 Statistical Analysis

The data are represented as mean+/− standard error of the mean. Unless indicated otherwise, a student's t-test was performed to determine statistical significance of results. A p value of < 0.01 (**) or <0.05 (*) was considered statistically significant.

3. RESULTS

3.1 Glucocorticoid receptors in the mouse cornea

To determine if the glucocorticoid receptor is present in the adult mouse cornea, glucocorticoid receptor expression was examined in 2 month-old wild type female mice by immunofluorescence. Nuclei in all layers of the cornea- the corneal epithelium, the stroma and the endothelium are stained positive for the glucocorticoid receptor (Figure 1). This data suggests that the glucocorticoid receptor may play a role in regulating the function of the adult cornea. Particularly interesting was the robust expression of the glucocorticoid receptor in all the cells of the corneal epithelium. To establish the functionality of GR in the mouse cornea, adult wild type female mice were treated with vehicle or dexamethasone eye drops and 6 hours later *Glucocorticoid-Induced Leucine Zipper (Gilz)* and *FK506 Binding protein 5 (Fkbp5),* the two classical target genes of glucocorticoid receptor signaling were quantified by RT-PCR. Glucocorticoid treatment induced the expression of *Gilz* (Fig1B) and *Fkbp5* (Fig1C) demonstrating the presence of an active glucocorticoid signaling system in the mouse cornea. In order to evaluate the function of the glucocorticoid receptor in the corneal epithelium, an immortalized human corneal epithelial cell line was utilized for subsequent studies.

3.2 Human corneal epithelial cells express a functional glucocorticoid receptor signaling system

Glucocorticoid effects on human corneal epithelial cells have been previously reported for a few target genes (16,20,21), however, the genome wide actions of glucocorticoids have not been established. To address this issue, we performed western blotting in immortalized human corneal epithelial cell line to first determine if glucocorticoid receptor is expressed (18). Our studies demonstrate that glucocorticoid receptors are expressed by human corneal epithelial cells (Figure 2A). Subsequently, we elucidated the ability of the glucocorticoid receptor to undergo translocation to the nucleus following ligand binding. HCE cells treated either with vehicle or 100nM dexamethasone for an hour were fixed and immunofluorescence was performed. Glucocorticoid treatment resulted in translocation of glucocorticoid receptor to the nucleus, which was otherwise mostly cytoplasmic in location (Figure 2B). In order to establish the functionality of GR in these cells, we treated HCE cells with different doses of dexamethasone (0, 1, 10, 100 and 1000nM) for 6 hours, followed by RT-PCR for the expression of *GILZ* mRNA. Glucocorticoid treatment resulted in a dose-dependent induction of *GILZ* expression (Figure 2C). Glucocorticoid-induced upregulation of *GILZ* is mediated via the glucocorticoid receptor, because GILZ induction was inhibited in the presence of RU486- a glucocorticoid receptor antagonist (Figure 2D). These data indicate that transcriptionally active glucocorticoid receptor is expressed by HCE cells.

3.3 Global gene expression changes induced by glucocorticoid treatment in HCE cells

Glucocorticoids are known to regulate numerous genes in a variety of tissues and cell types from rodents and humans (22-24), but very little is known about their genome wide actions in specific corneal cell types. For example, Liu et al have prepared primary corneal fibroblasts from male human donors and they found that very long-term dexamethasone treatment (16 hours) greatly altered both the gene and microRNA profiles in human corneal fibroblasts (25). To our knowledge, no such global gene expression studies have been performed on human corneal epithelial cells. Since cornea is a mixture of different cell types and because glucocorticoid regulation is known to work in a cell-type specific manner, we focused our studies on the human corneal epithelial cells. We performed whole-genome microarray on human corneal epithelial cells. HCE cells were treated with 100nM dexamethasone for only 6 hours. Glucocorticoids significantly altered the expression of 4439 genes expressed in HCE cells (Figure 3A). Of the significantly regulated genes, 2046 genes (about 46.1%) were upregulated, while 2393 genes (about 53.9%) were downregulated by glucocorticoid treatment (Figure 3B). Ingenuity Pathway Analysis software was used to elucidate the biological significance of the genetic signature elicited by dexamethasone-treatment of HCE cells. The predicted top-ranked biological functions regulated by glucocorticoids are cell movement (679 genes), cell growth and proliferation (1135 genes), cell development (1002 genes), cell death and survival (918 genes) and cell morphology (685 genes) (Figure 3C). These data suggest that glucocorticoid treatment alters expression of genes involved in migration, growth and trauma. Since injuries affecting the corneal epithelium are the most common types of eye injuries reported (26), and because glucocorticoids are commonly prescribed to suppress inflammation in an injured cornea, we focused our functional analysis on the repair process involved in wound healing. Analysis of the 679 cell movement associated genes indicates that 294 genes (43.3%) were up-regulated and 385 genes (56.7%) were downregulated by dexamethasone (Figure 3D and Table1). Based on the literature, a network of all the 679 genes encompasses different nodes of genes regulating diverse cellular functions related to cell movement.

During the process of wound healing, cells at the wounded edge remodel their cytoskeleton to form polarized membrane protrusions such as lamellipodia and filopodia and move towards closing the wound (27,28). The effect of dexamethasone on corneal cell lamellipodia and filopodia has not been clearly defined. Ingenuity Pathway Analysis identified that 45 genes associated with lamellipodia were regulated by dexamethasone treatment (Figure 3E and S.Table1). Out of these 45 genes, dexamethasone treatment upregulated 19 genes (42.2%) and 26 genes (57.8%) were repressed. Lamellipodia gene network generated using Ingenuity Pathway Analysis suggested Epidermal Growth Factor Receptor (EGFR) as the most important regulator of lamellipodia formation in the presence of glucocorticoids. Cell surface glycoprotein CD44 and a guanine-nucleotide-exchange factor VAV1 are also suggested to be playing an important role in glucocorticoid-mediated changes to lamellipodia. In addition, we also found that 55 genes associated with filopodia were regulated by dexamethasone treatment (Figure 3F and S.Table2). Of these 55 genes, dexamethasone treatment upregulated 21 genes (38.2%) and 34 genes (61.8%) were repressed. Filopodia gene network suggested that several growth factors such as Vascular Endothelial Growth Factor (VEGF), Fibroblast Growth Factor 2 (FGF2) and Connective

Tissue Growth Factor (CTGF) played a role in glucocorticoid-mediated changes to the filopodia. Also a part of wound healing is reestablishing epithelial integrity to maintain corneal epithelial barrier function. Therefore, we searched for genes involved in permeability using Ingenuity Pathway Analysis. Fifty genes involved in diseases and functions associated with permeability were regulated by dexamethasone (Figure 3G and S.Table3). Of these 50 genes, 16 genes were upregulated (32%) and 34 genes (68%) were repressed by dexamethasone. According to the Permeability Gene Network, the glucocorticoid receptor appears to be serving as the most active hub in regulating a large cohort of genes involved in permeability. Thus, glucocorticoid signaling is critical in regulating the genes associated in cell migration, cytoskeletal remodeling and permeability in human corneal epithelial cells.

3.4 Independent Validation of genes from the microarray

To independently validate the changes in gene expression observed by microarray, we measured glucocorticoid-regulated expression of four genes- *Tumor necrosis factor receptor super family 11b* (*TNFRSF11b)*, Brain derived neurotropic factor (BDNF), Epiregulin (EREG) and *Nerve Growth Factor (NGF)* by real-time RT-PCR from HCE RNA samples that came from experiments independent from those employed in the microarray studies. For this purpose, HCE cells were treated for 6 hours with vehicle, dexamethasone (100nM) and/or RU486 (1000nM) (Figure 4). IPA identified these four genes to be involved in cell movement (Figure 3D). NGF was identified to be playing a role not only in migration of cells but also in regulating cytoskeleton and epithelial integrity (Figure 3 D-G). Consistent with the microarray results, *TNFRSF11b, BDNF, EREG and NGF were* repressed by glucocorticoids and this repression was blunted upon treating the cells with a combination of glucocorticoids and RU486 or with RU486 alone. These findings illustrate some of the ways by which glucocorticoids regulate corneal wound healing is by repressing the expression of genes involved in regulating cell movement, cytoskeleton rearrangement and maintenance of epithelial integrity.

3.5 Glucocorticoids delay *in vitro* wound healing in HCE cells

To determine if the biological processes identified to be regulated by glucocorticoid by microarray analysis are functions involved in wound healing of HCE cells, we performed real-time wound healing scratch assays. Confluent monolayers of HCE cells were treated overnight with vehicle, dexamethasone (1000nM) or RU486 (10uM) or a combination of dexamethasone and RU486. Treated cells were scratched and images of the healing edges were taken every 30 mins for up to 30 hours. Wound closure was delayed with dexamethasone treatment (Figure 5A and Supplemental movie). Treatment with RU486 not only inhibited glucocorticoid-mediated delay, but also accelerated wound closure (Figure 5A and Supplemental movie). All treatment conditions, except dexamethasone revealed complete wound closure, which is represented in the images showing time-projection over 18 hours (Figure 5B). Quantification of the distance migrated by the wounded monolayer revealed that dexamethasone-treated monolayer migrated the least distance when compared to the other treatment conditions (Figure 5C). Consistently, the percent of the area of wound closure was decreased in dexamethasone treated HCE monolayer at the end of 18 hours (Figure 5D). Interestingly, proliferation and viability of HCE cells were not affected by

glucocorticoid treatment (Supplemental Figure 1). These observations are consistent with the IPA analysis and demonstrate that glucocorticoid treatment indeed delays *in vitro* wound healing of HCE cell monolayer. Our findings indicate that this effect of delayed migration is mediated by the glucocorticoid receptor since this function can be rescued by treatment with glucocorticoid receptor antagonist RU486.

3.6 Glucocorticoid treatment of HCE monolayer alters lamellipodia and filopodia formation

To understand if glucocorticoid-mediated regulation of cytoskeleton of HCE cells is contributing to the delay in migration of dexamethasone-treated cells, we evaluated the activity of lamellipodia along the wounded monolayer by quantifying the change in lamellipodia area in response to dexamethasone treatment. The data demonstrate that dexamethasone treatment decreases the activity of lamellipodia as seen by decrease in the change in lamellipodia area (less region in red in Figure 5E) compared to the vehicle treated cells (Figure 5 E and F). Additionally, quantification of the number of filopodia generated by “leader cells” along the wounded monolayer of HCE cells treated with glucocorticoids revealed fewer filopodia compared to the vehicle-treated cells (arrows in Figure 5E, and Figure 5G). These changes observed in the cytoskeleton of glucocorticoid-pre-treated cells within minutes after creating a scratch wound are indicative of a slowly migrating monolayer.

3.7 Glucocorticoids improve tight-junction protein organization and enhance barrier function

Based on the effects of glucocorticoids on migration of HCE cells, we wished to determine the role of GR on basal epithelial permeability and barrier function. We treated subconfluent cultures of HCE cells with vehicle or 100nM dexamethasone for either 6 hours or 24 hours and stained fixed cells for zonula occludens 1 (ZO-1), a protein that associates with the tight junctions on epithelial cells. Glucocorticoid treatment for as little as 6 hours had a strong recruitment of ZO-1 along the plasma membrane compared to the vehicle-treated cells. Subsequently, 24hour treatment of subconfluent cultures with dexamethasone resulted in greater ZO-1 distribution along the plasma membrane, compared to the vehicle treatment but not as robust as seen in cells treated with dexamethasone for 6 hours. The explanation for this observation is possibly due to the subconfluent culture continuing to establish cell-to-cell connections by reorganizing junctional proteins while growing to reach maximum confluency. A representative plasma membrane profile of ZO-1 staining intensity shows a peak in the intensity in the dexamethasone treated cells at both 6hr and 24hr treatment conditions (Figure 6A). Consistent with glucocorticoids influencing ZO-1 localization to the plasma membrane to form organized tight-junctions, the results from the permeability assay indicated that dexamethasone-treated cells formed a tighter epithelial barrier, thus allowing significantly lower amount of FITC dextran to permeate through the monolayer than the vehicle-treated cells (Figure 6B). These data indicate that glucocorticoids regulate epithelial tight junction proteins in subconfluent as well as confluent cultures to enhance epithelial barrier function.

4. DISCUSSION

Corticosteroids are widely used by ophthalmologists to treat various conditions of the cornea, but very little is known about their cell type specific actions in this tissue. In this study, we determined the expression pattern of the glucocorticoid receptor expression in an adult mouse cornea and we characterized the glucocorticoid receptor system using a human corneal epithelial cell line. Whole genome array results reveal an intricate dialogue between dexamethasone and HCE cells. We provide comprehensive analyses of the cellular and biological processes in corneal epithelial cells mediated by glucocorticoid treatment. The glucocorticoid transcriptome in HCE cells can serve as an important resource to the research community where it can be used to identify the targets to maximize the benefits and minimize the adverse affects of corticosteroid therapy. It is very important to note that our results were obtained using an immortalized human corneal epithelial cell line, which has been a tool widely used in ophthalmology for many years. However, recent studies have raised concerns regarding the differences between these immortalized HCE cells and primary human corneal epithelial cells in factors including inflammatory response (29), expression of atypical cytokeratins (30), purity of cell population (31), and the genomic content (31,32). Therefore, results from our in vitro studies may not precisely reflect the actions of glucocorticoids in primary human corneal epithelial cells.

Several of the genes altered in the microarray dataset have not been previously known to regulate cell movement in the various cell types of ocular tissues. For example, *TSC22D3* or *GILZ* is one of the most upregulated genes in the microarray dataset that have been previously reported to inhibit migration of leukocytes (33). *GILZ* gene expression has been shown to be induced by dexamethasone in the whole eye of a mouse (34), and in cultured primary human lens epithelial cells (35), but its expression or its role in the cornea has not been explored. Tumor necrosis factor receptor superfamily, member 11b (*TNFRSF11b*), a promoter of migration (36), is one of the most-repressed genes in this microarray dataset, which was reported to be expressed in corneal stroma (37), however its regulation by glucocorticoids in the cornea has never been reported. Comparison of the number of upregulated genes versus the downregulated genes from the microarray dataset suggested that glucocorticoid regulation of wound healing skewed towards downregulation of genes involved in promoting migration. An analysis using HCE cells to validate microarray results independent from the cells used for the global gene expression studies reveals that mRNA of *TNFRSF11b*, *BDNF, EREG* and *NGF* were indeed repressed by glucocorticoids and this repression was abolished by antagonism of the glucocorticoid receptor by the GR antagonist-RU486. TNFRSF11b (also known as Osteoprotegerin), a member of the TNF receptor super family is a secreted decoy receptor that has been associated with increase in bone density as a result of decrease in osteoclast-mediated bone resorption (38). Brain derived neurotropic factor (BDNF) is a member of the neurotrophin gene family with established roles in neuronal development and survival (39). Although BDNF's role in neurogenesis and cell survival has been well characterized (40), there are only a few studies investigating the function of BDNF in the cornea. For example, the presence of *BDNF* mRNA in the human cornea is potentially associated with proliferation of corneal epithelial cells, suggesting an important role for BDNF in corneal function (41). Repression of *BDNF*

gene expression is perhaps a novel mechanism exerted by glucocorticoids to regulate cell migration. Epiregulin (EREG) is a recently identified member of the epidermal growth factor family of ligands with functions in inflammation and wound healing (42). In mice, EREG is also known to play a critical role in corneal wound healing (43). A potential therapeutic strategy of co-administering glucocorticoids and epiregulin might offer a beneficial outcome in cases of corneal injury. Nerve growth factor (NGF) is the first-discovered member of the neurotrophin gene family, which is involved in the growth and survival of nerves (44). NGF in the cornea has been thought to play a role in promoting corneal nerve regeneration (45). In the context of wound healing, NGF is known to accelerate wound healing by promoting cell cycle progression and by increasing cell migration (46,47). A more recent study reports that NGF may have a negative impact on wound recovery by inhibiting regression of corneal lymphatic vessels and increasing the nerve density, thereby increasing sensitivity to pain (48). Glucocorticoids suppressing NGF during corneal wound healing could lead to be a better recovery of the wound, and with less pain. Interestingly, IPA identified NGF to be playing a role in cell movement, cytoskeletal reorganization and maintenance of epithelial barrier suggesting that glucocorticoids can modulate multiple biological processes driving wound healing by altering the expression of a single gene.

Corneal injuries are the most common cases of eye injury. Corneal wound healing is a complex physiological process that is modulated by a number of signaling pathways. Maintaining a protective barrier is one of the crucial functions of the corneal epithelium. We have investigated the effect of glucocorticoids on corneal wound healing in an *in vitro* model. This study demonstrates that glucocorticoids inhibit wound healing of human corneal epithelial cells by altering the activity of membrane lamellipodia and filopodia, together blunting the rate of migration. We also demonstrate that glucocorticoids enhance epithelial integrity by altering tight-junction protein distribution. Our data indicate that glucocorticoid-induced improvement of barrier function in subconfluent cultures can be relevant to the remodeling of a wounded epithelium. The results suggest that wound healing in the presence of glucocorticoids may result in a wound that heals at a slower rate, with improved epithelial integrity. Because epithelial integrity is an essential function in maintaining corneal homeostasis, delayed wound healing as an adverse outcome of glucocorticoid therapy does not seem entirely adverse since glucocorticoids promote improved tight junction integrity and thereby the enhanced epithelial barrier function.

Supplementary Material

Refer to Web version on PubMed Central for supplementary material.

ACKNOWLEDGMENT

We thank Jeff Tucker from the NIEHS Fluorescence Microscopy and Imaging Center for his assistance in the real-time wound healing studies. We also thank the NIEHS Flow Cytometry Center. We thank Drs. Robert Oakley, Xiaoling Li and Harriet Kinyamu for their critical reading of the manuscript. This work was funded by the NIEHS Intramural Research Program.

REFERENCES

1. Ren R, Oakley RH, Cruz-Topete D, Cidlowski JA. Dual role for glucocorticoids in cardiomyocyte hypertrophy and apoptosis. Endocrinology. 2012; 153:5346–5360. [PubMed: 22989630]
2. Gruver-Yates AL, Quinn MA, Cidlowski JA. Analysis of glucocorticoid receptors and their apoptotic response to dexamethasone in male murine B cells during development. Endocrinology. 2014; 155:463–474. [PubMed: 24196358]
3. Chang JH, Gabison EE, Kato T, Azar DT. Corneal neovascularization. Current opinion in ophthalmology. 2001; 12:242–249. [PubMed: 11507336]
4. Lambiase A, Abdolrahimzadeh S, Recupero SM. An update on intravitreal implants in use for eye disorders. Drugs of today. 2014; 50:239–249. [PubMed: 24696869]
5. Xie X, Yan X, Lin Z, Jin X. Differential effects of low- and high-dose glucocorticoids on the innate immunity of corneal epithelium in vitro. Ocul Immunol Inflamm. 2011; 19:275–281. [PubMed: 21770806]
6. Susarla R, Liu L, Walker EA, Bujalska IJ, Alsalem J, Williams GP, Sreekantam S, Taylor AE, Tallouzi M, Southworth HS, Murray PI, Wallace GR, Rauz S. Cortisol biosynthesis in the human ocular surface innate immune response. PLoS One. 2014; 9:e94913. [PubMed: 24736562]
7. Mirabelli P, Peebo BB, Xeroudaki M, Koulikovska M, Lagali N. Early effects of dexamethasone and anti-VEGF therapy in an inflammatory corneal neovascularization model. Experimental eye research. 2014; 125:118–127. [PubMed: 24933712]
8. Cardoso SS, Ferreira AL. Effect of adrenalectomy and of dexamethasone upon circadian distribution of mitosis in the cornea of rats. I. Proc Soc Exp Biol Med. 1967; 125:1254–1259. [PubMed: 6042438]
9. Pezuk P, Mohawk JA, Wang LA, Menaker M. Glucocorticoids as entraining signals for peripheral circadian oscillators. Endocrinology. 2012; 153:4775–4783. [PubMed: 22893723]
10. Ellenberg D, Azar DT, Hallak JA, Tobaigy F, Han KY, Jain S, Zhou Z, Chang JH. Novel aspects of corneal angiogenic and lymphangiogenic privilege. Progress in retinal and eye research. 2010; 29:208–248. [PubMed: 20100589]
11. Steele MM, Kelley PM, Schieler AM, Tempero RM. Glucocorticoids suppress corneal lymphangiogenesis. Cornea. 2011; 30:1442–1447. [PubMed: 21955630]
12. Saud EE, Moraes HV Jr. Marculino LG, Gomes JA, Allodi S, Miguel NC. Clinical and histopathological outcomes of subconjunctival triamcinolone injection for the treatment of acute ocular alkali burn in rabbits. Cornea. 2012; 31:181–187. [PubMed: 22081154]
13. A double-masked, placebo-controlled evaluation of 0.5% loteprednol etabonate in the treatment of postoperative inflammation. The Loteprednol Etabonate Postoperative Inflammation Study Group 2. Ophthalmology. 1998; 105:1780–1786. [PubMed: 9754192]
14. Bron A, Denis P, Hoang-Xuan TC, Boureau-Andrieux C, Crozafon P, Hachet E, Medhorn E, Akingbehin A. The effects of Rimexolone 1% in postoperative inflammation after cataract extraction. A double-masked placebo-controlled study. European journal of ophthalmology. 1998; 8:16–21. [PubMed: 9590590]
15. Bielory L. Ocular allergy treatment. Immunology and allergy clinics of North America. 2008; 28:189–224. vii. [PubMed: 18282552]
16. Kimura K, Teranishi S, Kawamoto K, Nishida T. Protective effect of dexamethasone against hypoxia-induced disruption of barrier function in human corneal epithelial cells. Experimental eye research. 2011; 92:388–393. [PubMed: 21354133]
17. Petroutsos G, Guimaraes R, Giraud JP, Pouliquen Y. Corticosteroids and corneal epithelial wound healing. The British journal of ophthalmology. 1982; 66:705–708. [PubMed: 6896993]
18. Araki-Sasaki K, Ohashi Y, Sasabe T, Hayashi K, Watanabe H, Tano Y, Handa H. An SV40-immortalized human corneal epithelial cell line and its characterization. Investigative ophthalmology & visual science. 1995; 36:614–621. [PubMed: 7534282]
19. Cidlowski JA, Bellingham DL, Powell-Oliver FE, Lubahn DB, Sar M. Novel antipeptide antibodies to the human glucocorticoid receptor: recognition of multiple receptor forms in vitro and distinct localization of cytoplasmic and nuclear receptors. Molecular endocrinology. 1990; 4:1427–1437. [PubMed: 1704480]

20. Seo KY, Chung SH, Lee JH, Park MY, Kim EK. Regulation of membrane-associated mucins in the human corneal epithelial cells by dexamethasone. Cornea. 2007; 26:709–714. [PubMed: 17592322]
21. Xie X, Yan X, Lin Z, Jin X. Differential effects of low- and high-dose glucocorticoids on the innate immunity of corneal epithelium in vitro. Ocular immunology and inflammation. 2011; 19:275–281. [PubMed: 21770806]
22. Duma D, Collins JB, Chou JW, Cidlowski JA. Sexually dimorphic actions of glucocorticoids provide a link to inflammatory diseases with gender differences in prevalence. Science signaling. 2010; 3:ra74. [PubMed: 20940427]
23. Oakley RH, Ren R, Cruz-Topete D, Bird GS, Myers PH, Boyle MC, Schneider MD, Willis MS, Cidlowski JA. Essential role of stress hormone signaling in cardiomyocytes for the prevention of heart disease. Proceedings of the National Academy of Sciences of the United States of America. 2013; 110:17035–17040. [PubMed: 24082121]
24. Revollo JR, Oakley RH, Lu NZ, Kadmiel M, Gandhavadi M, Cidlowski JA. HES1 is a master regulator of glucocorticoid receptor-dependent gene expression. Science signaling. 2013; 6:ra103. [PubMed: 24300895]
25. Liu L, Walker EA, Kissane S, Khan I, Murray PI, Rauz S, Wallace GR. Gene expression and miR profiles of human corneal fibroblasts in response to dexamethasone. Investigative ophthalmology & visual science. 2011; 52:7282–7288. [PubMed: 21666241]
26. McGwin G Jr. Owsley C. Incidence of emergency department-treated eye injury in the United States. Archives of ophthalmology. 2005; 123:662–666. [PubMed: 15883286]
27. Poujade M, Grasland-Mongrain E, Hertzog A, Jouanneau J, Chavrier P, Ladoux B, Buguin A, Silberzan P. Collective migration of an epithelial monolayer in response to a model wound. Proceedings of the National Academy of Sciences of the United States of America. 2007; 104:15988–15993. [PubMed: 17905871]
28. Omelchenko T, Vasiliev JM, Gelfand IM, Feder HH, Bonder EM. Rho-dependent formation of epithelial "leader" cells during wound healing. Proceedings of the National Academy of Sciences of the United States of America. 2003; 100:10788–10793. [PubMed: 12960404]
29. Suzuki T, Sullivan DA. Comparative effects of estrogen on matrix metalloproteinases and cytokines in immortalized and primary human corneal epithelial cell cultures. Cornea. 2006; 25:454–459. [PubMed: 16670485]
30. Huhtala A, Nurmi SK, Tahti H, Salminen L, Alajuuma P, Rantala I, Helin H, Uusitalo H. The immunohistochemical characterisation of an SV40-immortalised human corneal epithelial cell line. Altern Lab Anim. 2003; 31:409–417. [PubMed: 15601246]
31. Yamasaki K, Kawasaki S, Young RD, Fukuoka H, Tanioka H, Nakatsukasa M, Quantock AJ, Kinoshita S. Genomic aberrations and cellular heterogeneity in SV40-immortalized human corneal epithelial cells. Invest Ophthalmol Vis Sci. 2009; 50:604–613. [PubMed: 18824731]
32. Greco D, Vellonen KS, Turner HC, Hakli M, Tervo T, Auvinen P, Wolosin JM, Urtti A. Gene expression analysis in SV-40 immortalized human corneal epithelial cells cultured with an air-liquid interface. Mol Vis. 2010; 16:2109–2120. [PubMed: 21139686]
33. Mazzon E, Bruscoli S, Galuppo M, Biagioli M, Sorcini D, Bereshchenko O, Fiorucci C, Migliorati G, Bramanti P, Riccardi C. Glucocorticoid-induced leucine zipper (GILZ) controls inflammation and tissue damage after spinal cord injury. CNS neuroscience & therapeutics. 2014; 20:973–981. [PubMed: 25146427]
34. Cari L, Ricci E, Gentili M, Petrillo MG, Ayroldi E, Ronchetti S, Nocentini G, Riccardi C. A focused Real Time PCR strategy to determine GILZ expression in mouse tissues. Results Immunol. 2015; 5:37–42. [PubMed: 26697291]
35. Gupta V, Galante A, Soteropoulos P, Guo S, Wagner BJ. Global gene profiling reveals novel glucocorticoid induced changes in gene expression of human lens epithelial cells. Mol Vis. 2005; 11:1018–1040. [PubMed: 16319822]
36. Kobayashi-Sakamoto M, Isogai E, Hirose K, Chiba I. Role of alphav integrin in osteoprotegerin-induced endothelial cell migration and proliferation. Microvascular research. 2008; 76:139–144. [PubMed: 18656492]

37. Wilson SE, Mohan RR, Netto M, Perez V, Possin D, Huang J, Kwon R, Alekseev A, Rodriguez-Perez JP. RANK, RANKL, OPG, and M-CSF expression in stromal cells during corneal wound healing. Investigative ophthalmology & visual science. 2004; 45:2201–2211. [PubMed: 15223796]

38. Simonet WS, Lacey DL, Dunstan CR, Kelley M, Chang MS, Luthy R, Nguyen HQ, Wooden S, Bennett L, Boone T, Shimamoto G, DeRose M, Elliott R, Colombero A, Tan HL, Trail G, Sullivan J, Davy E, Bucay N, Renshaw-Gegg L, Hughes TM, Hill D, Pattison W, Campbell P, Sander S, Van G, Tarpley J, Derby P, Lee R, Boyle WJ. Osteoprotegerin: a novel secreted protein involved in the regulation of bone density. Cell. 1997; 89:309–319. [PubMed: 9108485]

39. Bhave SV, Ghoda L, Hoffman PL. Brain-derived neurotrophic factor mediates the anti-apoptotic effect of NMDA in cerebellar granule neurons: signal transduction cascades and site of ethanol action. J Neurosci. 1999; 19:3277–3286. [PubMed: 10212287]

40. Chao MV, Rajagopal R, Lee FS. Neurotrophin signalling in health and disease. Clinical science. 2006; 110:167–173. [PubMed: 16411893]

41. You L, Kruse FE, Volcker HE. Neurotrophic factors in the human cornea. Investigative ophthalmology & visual science. 2000; 41:692–702. [PubMed: 10711683]

42. Riese DJ 2nd, Cullum RL. Epiregulin: roles in normal physiology and cancer. Semin Cell Dev Biol. 2014; 28:49–56. [PubMed: 24631357]

43. Zhang Y, Kobayashi T, Hayashi Y, Yoshioka R, Shiraishi A, Shirasawa S, Higashiyama S, Ohashi Y. Important role of epiregulin in inflammatory responses during corneal epithelial wound healing. Investigative ophthalmology & visual science. 2012; 53:2414–2423. [PubMed: 22427548]

44. Cohen S, Levi-Montalcini R, Hamburger V. A Nerve Growth-Stimulating Factor Isolated from Sarcom as 37 and 180. Proc Natl Acad Sci U S A. 1954; 40:1014–1018. [PubMed: 16589582]

45. Sarkar J, Chaudhary S, Jassim SH, Ozturk O, Chamon W, Ganesh B, Tibrewal S, Gandhi S, Byun YS, Hallak J, Mahmud DL, Mahmud N, Rondelli D, Jain S. CD11b+GR1+ myeloid cells secrete NGF and promote trigeminal ganglion neurite growth: implications for corneal nerve regeneration. Invest Ophthalmol Vis Sci. 2013; 54:5920–5936. [PubMed: 23942970]

46. Hong J, Qian T, Le Q, Sun X, Wu J, Chen J, Yu X, Xu J. NGF promotes cell cycle progression by regulating D-type cyclins via PI3K/Akt and MAPK/Erk activation in human corneal epithelial cells. Mol Vis. 2012; 18:758–764. [PubMed: 22509106]

47. Blanco-Mezquita T, Martinez-Garcia C, Proenca R, Zieske JD, Bonini S, Lambiase A, Merayo-Lloves J. Nerve growth factor promotes corneal epithelial migration by enhancing expression of matrix metalloprotease-9. Invest Ophthalmol Vis Sci. 2013; 54:3880–3890. [PubMed: 23640040]

48. Fink DM, Connor AL, Kelley PM, Steele MM, Hollingsworth MA, Tempero RM. Nerve growth factor regulates neurolymphatic remodeling during corneal inflammation and resolution. PLoS One. 2014; 9:e112737. [PubMed: 25383879]

HIGHLIGHTS

- Functional glucocorticoid receptors are expressed in mouse corneas.
- Glucocorticoids regulated over 4000 genes in human corneal epithelial cells.
- Glucocorticoids enriched genes associated in wound healing processes.
- Glucocorticoids decreased cell migration rate but enhanced epithelial integrity.

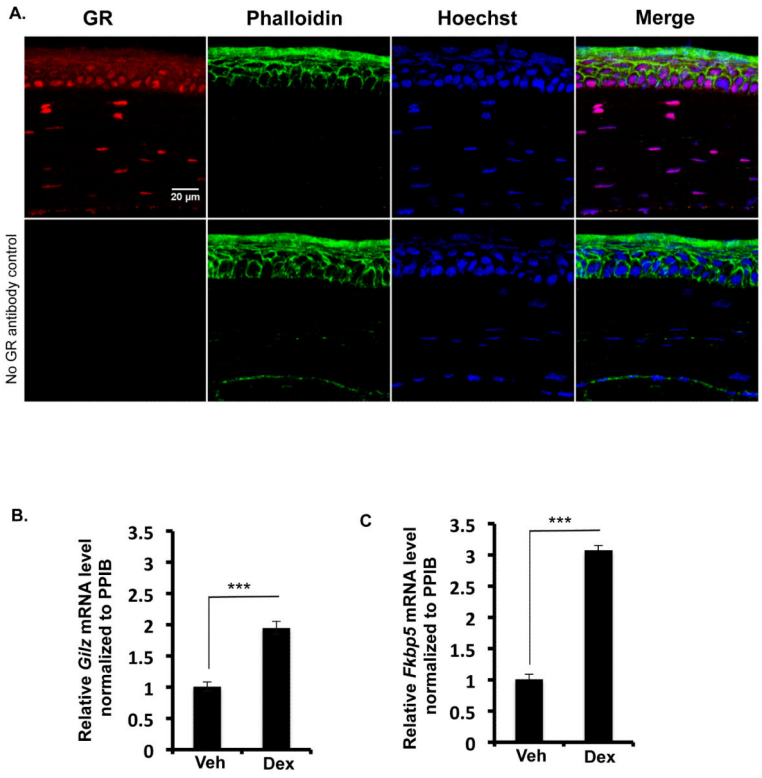

Figure 1.

Glucocorticoid Receptor signaling in the adult mouse cornea. A) Immunofluorescence of wild type adult female mouse cornea showing glucocorticoid receptor expression (red) in all the layers of the corneal epithelium, in the corneal stromal cells and in the corneal endothelial cells. Phalloidin and Hoechst were used to visualize actin (green) and nuclei (blue), respectively. A merge of all three channels is presented in the fourth panel. Scale bar: 20μm. B) & C) Adrenalectomized wild type mice were treated for 6 hours with vehicle or dexamethasone eye drops and *GILZ* mRNA (B) and *FKBP5* mRNA (C) were evaluated by quantitative RT-PCR. Results were normalized to *PPIB* gene expression (housekeeping gene). Data represent mean ± standard error of mean from four biological replicates. Student's t-test was used to determine statistical significance compared to the vehicle-treated cells; *** $p<0.001$.

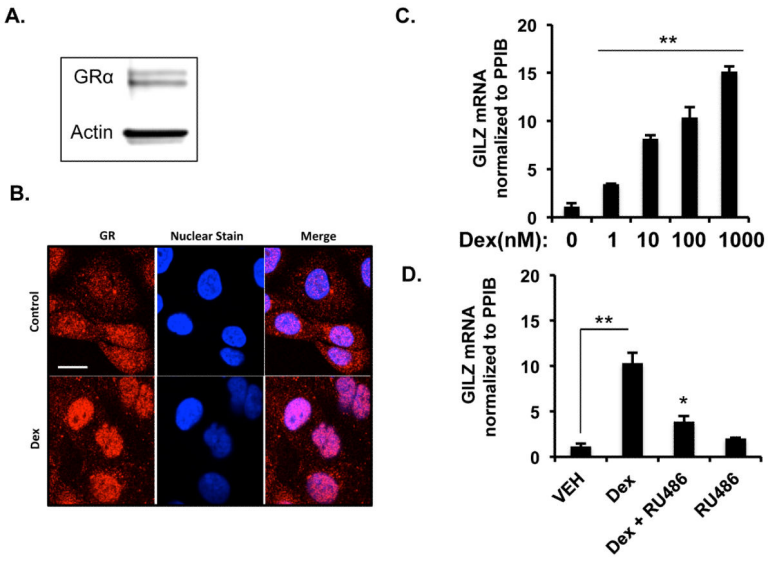

Figure 2.

Corneal epithelial cells express functional glucocorticoid receptors. A) Glucocorticoid receptor protein level expressed by immortalized human corneal epithelial (HCE) cells evaluated by immunoblot. Actin was used as the loading control. B) Nuclear translocation of glucocorticoid receptor by immunofluorescence in HCE cells treated with 100nM dexamethasone for 1 hour at 37 degrees centigrade. Glucocorticoid receptor expression is in red and Hoechst staining of the nuclei is in blue. C) HCE cells were treated with vehicle or four different concentrations of dexamethasone for 6hrs and GILZ mRNA was measure by quantitative RT-PCR. D) HCE cells were treated for 6 hours with vehicle, dexamethasone (100nM), RU486- an antagonist of glucocorticoid receptor (1000nM), or both and *GILZ* mRNA was evaluated by quantitative RT-PCR. Results were normalized to *PPIB* gene expression (housekeeping gene). Data represent mean ± standard error of mean from three or four independent experiments. Student's t-test was used to determine statistical significance compared to the vehicle-treated cells; * $p<0.05$ and ** $p<0.01$.

A.

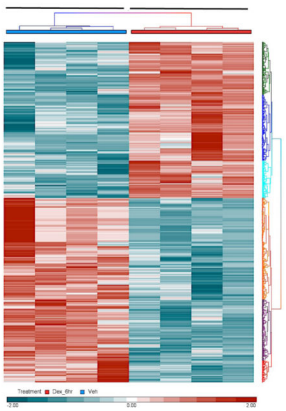

B.

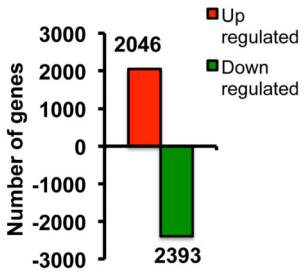

C.

Top Biological Functions		
Molecular & Cellular Functions	**# of genes**	**p-value**
1. Cell Movement	679	1.27E-06 – 3.19E-33
2. Cell Growth and Proliferation	1135	1.29E-06 – 1.71E-30
3. Cell Development	1002	1.29E-06 – 1.37E-23
4. Cell Death and Survival	918	1.06E-06 – 6.23E-23
5. Cell Morphology	685	8.41E-07 – 8.03E-21

D. Cell Movement gene network

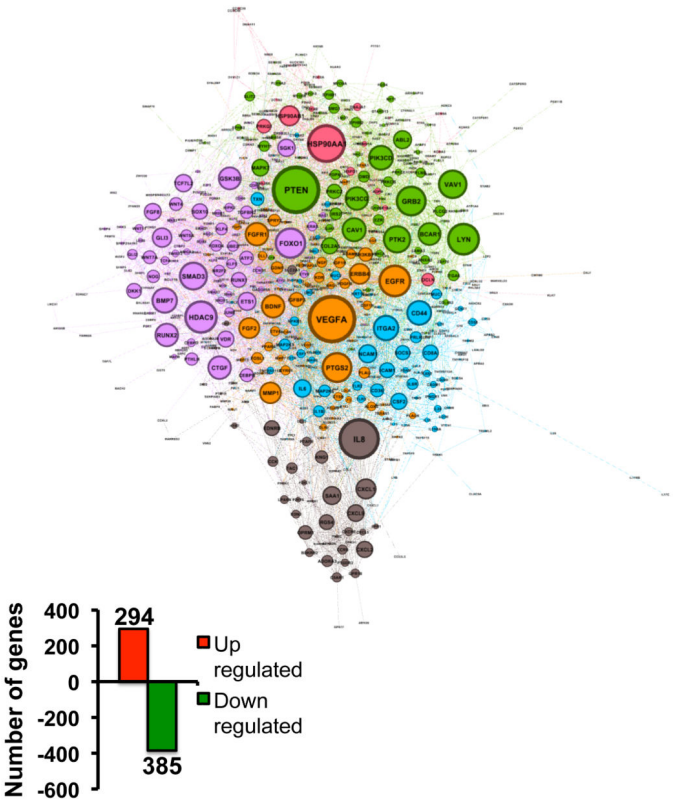

E. Lamellipodia gene network

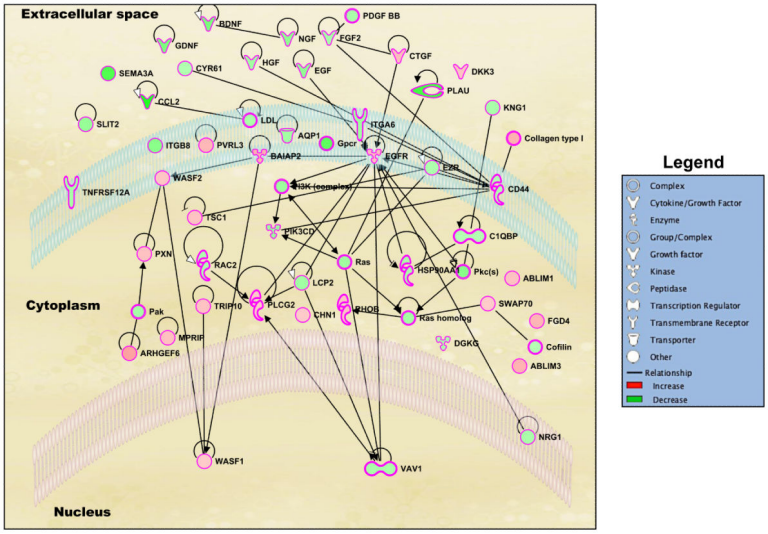

F. Filopodia gene network

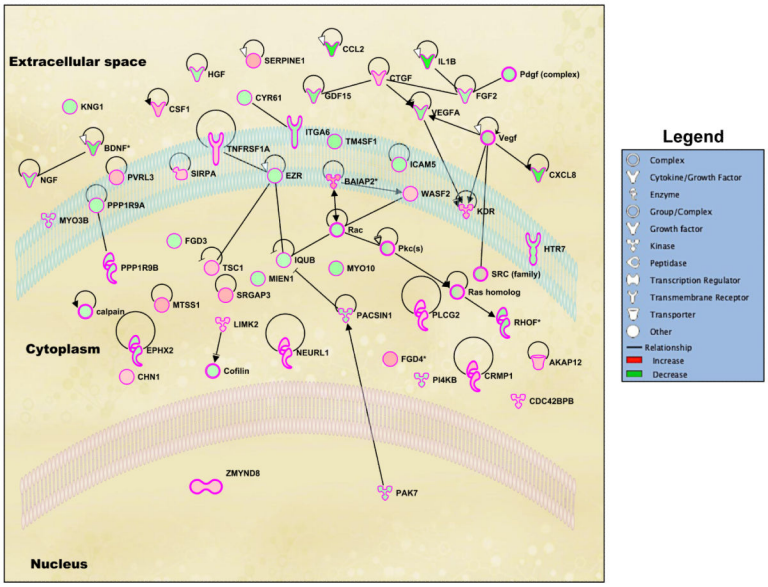

G. Permeability gene network

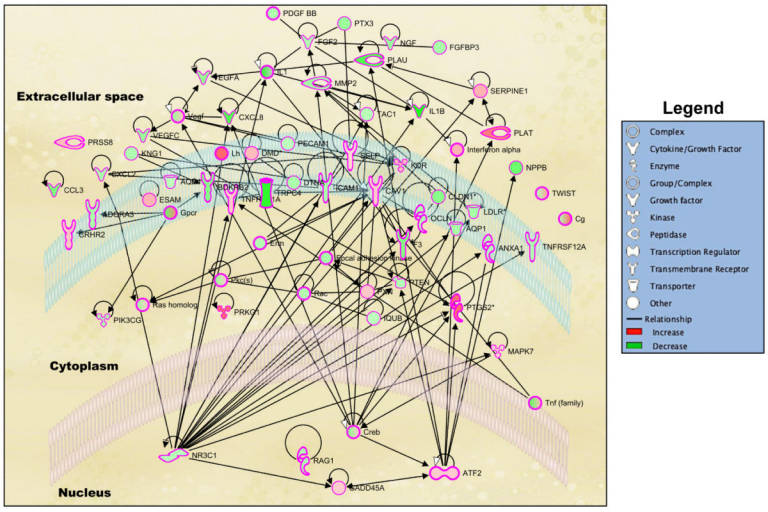

Figure 3.

Genome-wide regulation by glucocorticoids in HCE cells. HCE cells were treated with vehicle or 100nM dexamethasone (Dex). RNA was isolated and gene expression was analyzed using whole mouse genome 4×44 multiplex format Aglient oligo array. A) Heat map of genes regulated significantly by 100nM dexamethasone in 6 hours (ANOVA $p<0.01$); Red represents upregulated genes and blue represents downregulated genes in each of the 4 replicates/group. B) Bar-graph is representing glucocorticoid-regulated genes in red (upregulated) and in green (downregulated). C) Glucocorticoid-regulated gene list from HCE cells obtained by microarray were analyzed using Ingenuity Pathway Analysis (IPA) software. IPA predicted glucocorticoid treatment to regulate several molecular and cellular

functions, of which the top 5 are listed in the table; Cell movement was ranked as the top most molecular and cellular function regulated by glucocorticoids in HCE cells. D) Gene network of Cell Movement genes identifying different nodes of genes regulating various cellular functions associated with cellular movement; Bar-graph is representing glucocorticoid-regulated cell movement genes in red (upregulated, 294 genes) and in green (downregulated, 385 genes). E-G) Glucocorticoid-regulated genes associated in diseases and functions involving lamellipodia (E), filopodia (F) and permeability (G). Green indicates repression and red indicates upregulation of gene expression; A family of genes with some members upregulated and some members downregulated are indicated in both green and red. The black lines/arrows indicate direct interaction either at the gene/protein level as indicated by Ingenuity Pathway Analysis.

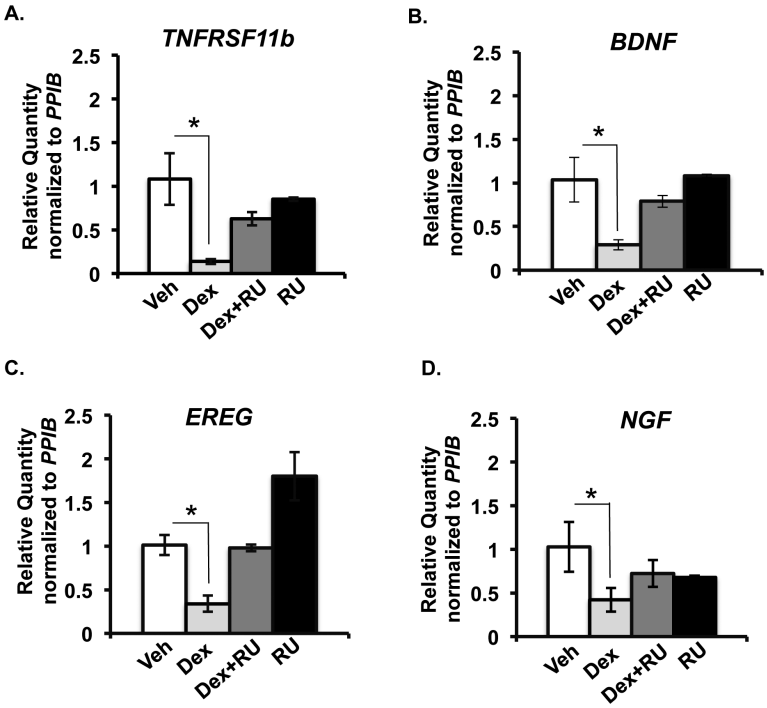

Figure 4.

Validation of microarray results by RT-PCR. *TNFRSF11b*, *BDNF*, *EREG and NGF* mRNA levels measured by RT-PCR and normalized to *PPIB* mRNA level in HCE cells treated with vehicle (white bars) or 100 nM dexamethasone (light grey bars) or a combination of 100nM dexamethasone and 1000nM RU486 (dark grey bars) or 1000nM RU486 (black bars). n = 3 or 4 biological replicates; *$p<0.05$.

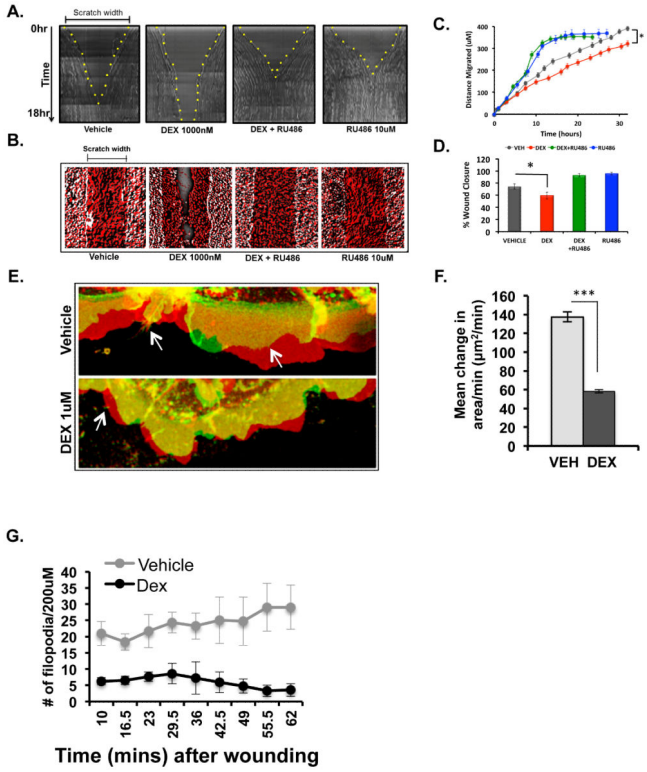

Figure 5.

Glucocorticoids delay in vitro wound healing of HCE cells. Scratch assay was performed on confluent monolayers of cells pre-treated overnight alone or in combination with vehicle, DEX (1000nM), or RU486 (10uM) in charcoal-stripped serum containing medium. Real-time analysis of cell migration was performed by imaging the every 30 minutes for 18 hours post-scratch. A) Representative images of wound healing kinetics in all the 4 conditions-vehicle, dexamethasone (1000nM), combination of dexamethasone (1000nM) and RU486 (10uM) and RU 486 (10uM) alone. Scratch width and time are on the X- and Y- axes, respectively. Yellow dots indicate the edge of the scratched monolayer. B) Representative images showing the time-projection of wound healing over a period of 18 hours in all four conditions. Time-projection is indicated with t0 in white and t18hrs in red. C) Quantification of the extent of wound healing measured from time-lapse images taken over a period of 30 hours. Average of four individual experiments is represented here (*$p<0.001$). D) Average area of wound closure in 18 hours represented in percentage from four individual experiments (*$p<0.05$). E) Representative images showing the net change in the area of the lamellipodia in vehicle and dexamethasone (1000nM) treated cells at 30 minutes after scratching the monolayer. Red represents lamellipodia that are moving forward to close the wound, green represents retraction of the lamellipodia and yellow represents no change in net movement of the lamellipodia over a period of approximately 6 minutes. Arrows are pointing to the filopodia. F) Average of the change in the area of the lamellipodia per minute in 10 minutes after creating a scratch wound in the monolayer in HCE cells treated overnight with either vehicle or 1000nM dexamethasone. Results from three experiments were averaged and are shown here. G) Average number of filopodia formed at the wounded

monolayer between 10-65 minutes of wound healing. An average of three individual experiments is represented here.

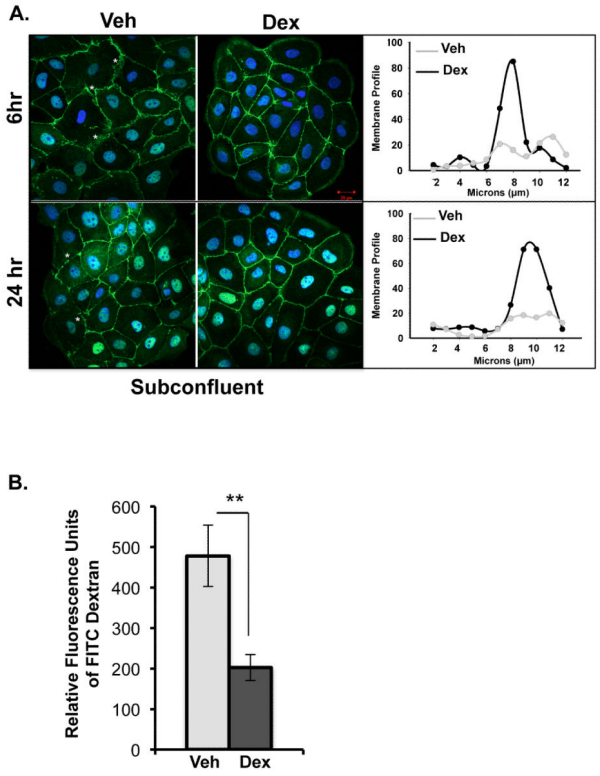

Figure 6.

Glucocorticoids regulate ZO-1 distribution and epithelial permeability. A) Immunofluorescence of subconfluent cultures of HCE cells exhibiting ZO-1 distribution in vehicle or 1uM dexamethasone for either 6 hours or 24 hours. Asterisks indicate site of disorganized ZO-1 staining. Images are maximum intensity projections of Z-stacks imaged through the entire depth of the cell membrane. Images are a merge of Hoechst staining (blue) and ZO-1 staining (green). A representative plasma membrane profile of ZO-1 staining intensity shows a peak in the intensity in the dexamethasone treated cells (black line) at both 6hr and 24hr treatment conditions. B) Relative changes in permeability were determined by measuring the fluorescence unit of FITC dextran that permeated through the epithelial monolayer in cells treated for 24hours either with vehicle or 100nM dexamethasone. An average of three independent experiments is represented here. **p value < 0.01.

Table 1

Dexamethasone regulation of genes associated in cell movement

Up regulated genes

Number	Symbol	Entrez Gene Name	Fold Change
1	PDE2A	phosphodiesterase 2A	9.80859
2	TSC22D3	TSC22 domain family member 3	8.37242
3	ALOX5AP	arachidonate 5-lipoxygenase-activating protein	5.66178
4	FAM65B	family with sequence similarity 65 member B	4.66935
5	PER1	period circadian clock 1	4.65227
6	KLF6	Kruppel-like factor 6	4.38594
7	MMP7	matrix metallopeptidase 7	4.25261
8	ERBB4	erb-b2 receptor tyrosine kinase 4	3.90165
9	EDN2	endothelin 2	3.82819
10	PRKG1	protein kinase, cGMP-dependent, type I	3.7749
11	CGA	glycoprotein hormones, alpha polypeptide	3.76295
12	DMBT1	deleted in malignant brain tumors 1	3.72217
13	PTGS2	prostaglandin-endoperoxide synthase 2 (prostaglandin G/H synthase and cyclooxygenase)	3.6601
14	FGF8	fibroblast growth factor 8	3.36341
15	PLAT	plasminogen activator, tissue type	3.26515
16	TREM1	triggering receptor expressed on myeloid cells 1	3.25299
17	FAM43A	family with sequence similarity 43 member A	3.07726
18	TLR2	toll-like receptor 2	3.05242
19	COL4A3	collagen, type IV, alpha 3 (Goodpasture antigen)	2.91731
20	ACKR3	atypical chemokine receptor 3	2.91065
21	CCBE1	collagen and calcium binding EGF domains 1	2.89472
22	IGK	immunoglobulin kappa locus	2.77607
23	GCNT1	glucosaminyl (N-acetyl) transferase 1, core 2	2.72011
24	FFAR4	free fatty acid receptor 4	2.71943
25	BMP7	bone morphogenetic protein 7	2.63977
26	SCNN1A	sodium channel, non voltage gated 1 alpha subunit	2.601
27	MAFB	v-maf avian musculoaponeurotic fibrosarcoma oncogene homolog B	2.59413
28	C2	complement component 2	2.56885
29	RGCC	regulator of cell cycle	2.5588
30	ZAP70	zeta chain of T cell receptor associated protein kinase 70kDa	2.52303
31	PDIA2	protein disulfide isomerase family A member 2	2.52092
32	PTGES	prostaglandin E synthase	2.49236
33	G6PC	glucose-6-phosphatase, catalytic subunit	2.47483
34	WNT11	wingless-type MMTV integration site family member 11	2.45361

Number	Symbol	Entrez Gene Name	Fold Change
35	ERRFI1	ERBB receptor feedback inhibitor 1	2.42978
36	LMO7	LIM domain 7	2.42814
37	TWIST1	twist family bHLH transcription factor 1	2.39978
38	SERPINA5	serpin peptidase inhibitor, clade A (alpha-1 antiproteinase, antitrypsin), member 5	2.39942
39	EDNRB	endothelin receptor type B	2.39193
40	GP1BA	glycoprotein Ib platelet alpha subunit	2.38223
41	SFRP5	secreted frizzled-related protein 5	2.3733
42	KCNH2	potassium channel, voltage gated eag related subfamily H, member 2	2.33941
43	ST8SIA2	ST8 alpha-N-acetyl-neuraminide alpha-2,8-sialyltransferase 2	2.31557
44	PTGER2	prostaglandin E receptor 2	2.3143
45	TDGF1	teratocarcinoma-derived growth factor 1	2.31039
46	TREM2	triggering receptor expressed on myeloid cells 2	2.30895
47	BARX2	BARX homeobox 2	2.29272
48	TNS4	tensin 4	2.2516
49	SDR9C7	short chain dehydrogenase/reductase family 9C, member 7	2.24862
50	SOX10	SRY-box 10	2.23462
51	NME8	NME/NM23 family member 8	2.22648
52	HYAL1	hyaluronoglucosaminidase 1	2.22431
53	SFRP2	secreted frizzled-related protein 2	2.22094
54	ANXA2	annexin A2	2.21004
55	CSF1R	colony stimulating factor 1 receptor	2.20717
56	MYCN	v-myc avian myelocytomatosis viral oncogene neuroblastoma derived homolog	2.18662
57	PNOC	prepronociceptin	2.18369
58	POU3F2	POU class 3 homeobox 2	2.14487
59	LHX6	LIM homeobox 6	2.13937
60	NCAM1	neural cell adhesion molecule 1	2.12964
61	UNC5C	unc-5 netrin receptor C	2.12805
62	SAA1	serum amyloid A1	2.12535
63	ARHGEF6	Rac/Cdc42 guanine nucleotide exchange factor 6	2.12256
64	SEPT4	septin 4	2.09427
65	SEMA6D	semaphorin 6D	2.08409
66	AHSG	alpha-2-HS-glycoprotein	2.04678
67	FOXO4	forkhead box O4	2.03975
68	DUSP1	dual specificity phosphatase 1	2.03074
69	PIGR	polymeric immunoglobulin receptor	2.02612
70	CSPG4	chondroitin sulfate proteoglycan 4	2.02415
71	SERPINA3	serpin peptidase inhibitor, clade A (alpha-1 antiproteinase, antitrypsin), member 3	2.02111
72	FGD4	FYVE, RhoGEF and PH domain containing 4	2.01625

Number	Symbol	Entrez Gene Name	Fold Change
73	DACT2	dishevelled-binding antagonist of beta-catenin 2	1.99964
74	OVOL2	ovo-like zinc finger 2	1.99502
75	HTRA3	HtrA serine peptidase 3	1.98175
76	LOX	lysyl oxidase	1.96085
77	SNAI2	snail family zinc finger 2	1.95867
78	ST3GAL3	ST3 beta-galactoside alpha-2,3-sialyltransferase 3	1.95677
79	DKK1	dickkopf WNT signaling pathway inhibitor 1	1.95068
80	CAV3	caveolin 3	1.93759
81	PDPK1	3-phosphoinositide dependent protein kinase 1	1.93146
82	SGK1	serum/glucocorticoid regulated kinase 1	1.92796
83	CX3CL1	chemokine (C-X3-C motif) ligand 1	1.90246
84	RECK	reversion-inducing-cysteine-rich protein with kazal motifs	1.90193
85	TAF7L	TATA-box binding protein associated factor 7 like	1.89943
86	CXCL9	chemokine (C-X-C motif) ligand 9	1.89439
87	SERPINE1	serpin peptidase inhibitor, clade E (nexin, plasminogen activator inhibitor type 1), member 1	1.89231
88	ESAM	endothelial cell adhesion molecule	1.8895
89	MUC2	mucin 2, oligomeric mucus/gel-forming	1.88395
90	CCKBR	cholecystokinin B receptor	1.88322
91	MTSS1	metastasis suppressor 1	1.87278
92	SRCIN1	SRC kinase signaling inhibitor 1	1.87237
93	SCNN1G	sodium channel, non voltage gated 1 gamma subunit	1.87131
94	GUCY1A3	guanylate cyclase 1, soluble, alpha 3	1.86393
95	BCAN	brevican	1.84483
96	MMP28	matrix metallopeptidase 28	1.84228
97	A4GALT	alpha 1,4-galactosyltransferase	1.83856
98	ARRDC3	arrestin domain containing 3	1.82678
99	IL17C	interleukin 17C	1.80878
100	TNFRSF18	tumor necrosis factor receptor superfamily member 18	1.80542
101	LMCD1	LIM and cysteine-rich domains 1	1.79297
102	APBB2	amyloid beta (A4) precursor protein-binding, family B, member 2	1.78296
103	GPR173	G protein-coupled receptor 173	1.76787
104	CD22	CD22 molecule	1.7662
105	ARID5B	AT-rich interaction domain 5B	1.76014
106	COL2A1	collagen, type II, alpha 1	1.73823
107	TREML2	triggering receptor expressed on myeloid cells like 2	1.72252
108	CBLB	Cbl proto-oncogene B, E3 ubiquitin protein ligase	1.71418
109	DMD	dystrophin	1.70442
110	PTGDR2	prostaglandin D2 receptor 2	1.6963
111	CSF1	colony stimulating factor 1	1.69629

Number	Symbol	Entrez Gene Name	Fold Change
112	DEFB1	defensin beta 1	1.69534
113	AHNAK	AHNAK nucleoprotein	1.69458
114	ALPPL2	alkaline phosphatase, placental like 2	1.69249
115	ITGB6	integrin subunit beta 6	1.69233
116	KDR	kinase insert domain receptor	1.69116
117	NFKBIA	nuclear factor of kappa light polypeptide gene enhancer in B-cells inhibitor, alpha	1.68325
118	THBD	thrombomodulin	1.68252
119	DSG3	desmoglein 3	1.68104
120	IL6R	interleukin 6 receptor	1.67241
121	AZGP1	alpha-2-glycoprotein 1, zinc-binding	1.67019
122	CKLF	chemokine-like factor	1.6601
123	FABP5	fatty acid binding protein 5 (psoriasis-associated)	1.65888
124	DNAJB4	DnaJ heat shock protein family (Hsp40) member B4	1.65114
125	STAB2	stabilin 2	1.64157
126	GUCY1B3	guanylate cyclase 1, soluble, beta 3	1.64096
127	STAB1	stabilin 1	1.6352
128	HOXC9	homeobox C9	1.63051
129	KRT6B	keratin 6B, type II	1.61929
130	IL6ST	interleukin 6 signal transducer	1.61917
131	GGT5	gamma-glutamyltransferase 5	1.61518
132	PTH1R	parathyroid hormone 1 receptor	1.61329
133	FOXO1	forkhead box O1	1.6106
134	OPRD1	opioid receptor, delta 1	1.61012
135	TNFSF8	tumor necrosis factor superfamily member 8	1.60148
136	TG	thyroglobulin	1.59772
137	GNAQ	guanine nucleotide binding protein (G protein), q polypeptide	1.59632
138	MYO9A	myosin IXA	1.58634
139	TXNDC2	thioredoxin domain containing 2 (spermatozoa)	1.57836
140	WNT5A	wingless-type MMTV integration site family member 5A	1.56678
141	ROR1	receptor tyrosine kinase-like orphan receptor 1	1.56674
142	CRMP1	collapsin response mediator protein 1	1.55331
143	ATF3	activating transcription factor 3	1.55296
144	NTF4	neurotrophin 4	1.54373
145	C5AR2	complement component 5a receptor 2	1.54316
146	CD209	CD209 molecule	1.54084
147	TGFBR2	transforming growth factor beta receptor II	1.53985
148	HLA-G	major histocompatibility complex, class I, G	1.53451
149	CDH4	cadherin 4	1.5343
150	SPARCL1	SPARC like 1	1.53001

Number	Symbol	Entrez Gene Name	Fold Change
151	SFTPA1	surfactant protein A1	1.52362
152	FAP	fibroblast activation protein alpha	1.51341
153	MUC1	mucin 1, cell surface associated	1.50915
154	HIPK2	homeodomain interacting protein kinase 2	1.50556
155	LAMA3	laminin subunit alpha 3	1.50543
156	ADGRL3	adhesion G protein-coupled receptor L3	1.50267
157	NDRG1	N-myc downstream regulated 1	1.5009
158	DNAH11	dynein, axonemal, heavy chain 11	1.49615
159	HTRA1	HtrA serine peptidase 1	1.49229
160	DKK3	dickkopf WNT signaling pathway inhibitor 3	1.48976
161	IRX2	iroquois homeobox 2	1.48728
162	AKAP12	A-kinase anchoring protein 12	1.48594
163	CD8A	CD8a molecule	1.48588
164	CTGF	connective tissue growth factor	1.47837
165	PROK1	prokineticin 1	1.47053
166	MAVS	mitochondrial antiviral signaling protein	1.46925
167	IRS2	insulin receptor substrate 2	1.46551
168	ATP2B4	ATPase, Ca++ transporting, plasma membrane 4	1.46535
169	SEMA5A	semaphorin 5A	1.46424
170	AFAP1L1	actin filament associated protein 1 like 1	1.46064
171	MAPT	microtubule associated protein tau	1.45851
172	FOSL2	FOS like antigen 2	1.45689
173	NFIA	nuclear factor I/A	1.45523
174	EGFR	epidermal growth factor receptor	1.44947
175	ST3GAL4	ST3 beta-galactoside alpha-2,3-sialyltransferase 4	1.4478
176	ALPP	alkaline phosphatase, placental	1.44571
177	TUBB2B	tubulin beta 2B class IIb	1.4385
178	NTN1	netrin 1	1.43575
179	CXCL5	chemokine (C-X-C motif) ligand 5	1.43458
180	CRYAB	crystallin alpha B	1.43261
181	PLD1	phospholipase D1	1.42163
182	CD59	CD59 molecule	1.42106
183	KLF4	Kruppel-like factor 4 (gut)	1.41722
184	VNN2	vanin 2	1.41559
185	PLXNA2	plexin A2	1.40612
186	CMA1	chymase 1, mast cell	1.40552
187	SLC30A4	solute carrier family 30 (zinc transporter), member 4	1.40175
188	UNC5B	unc-5 netrin receptor B	1.39967
189	MARVELD	MARVEL domain containing 3	1.3954
190	ABLIM1	actin binding LIM protein 1	1.39124

Number	Symbol	Entrez Gene Name	Fold Change
191	FBLIM1	filamin binding LIM protein 1	1.39083
192	JUNB	jun B proto-oncogene	1.38982
193	KLF8	Kruppel-like factor 8	1.38587
194	CHRNA7	cholinergic receptor, nicotinic alpha 7	1.38155
195	ITGB7	integrin subunit beta 7	1.37875
196	ROBO3	roundabout guidance receptor 3	1.37754
197	PXN	paxillin	1.37578
198	CTSC	cathepsin C	1.37552
199	FLNB	filamin B	1.37067
200	CAMK2G	calcium/calmodulin-dependent protein kinase II gamma	1.36898
201	GPC1	glypican 1	1.36368
202	TRIP10	thyroid hormone receptor interactor 10	1.36183
203	GLI3	GLI family zinc finger 3	1.35695
204	PDCD4	programmed cell death 4 (neoplastic transformation inhibitor)	1.35597
205	TSC1	tuberous sclerosis 1	1.35562
206	IL15	interleukin 15	1.35092
207	TNFRSF1A	tumor necrosis factor receptor superfamily member 1A	1.34708
208	GLI2	GLI family zinc finger 2	1.34616
209	DAB2	Dab, mitogen-responsive phosphoprotein, homolog 2 (Drosophila)	1.3451
210	CEBPD	CCAAT/enhancer binding protein delta	1.34448
211	NOD1	nucleotide binding oligomerization domain containing 1	1.34023
212	RHOB	ras homolog family member B	1.33951
213	PDLIM1	PDZ and LIM domain 1	1.33705
214	ALOX15	arachidonate 15-lipoxygenase	1.33616
215	GPR161	G protein-coupled receptor 161	1.33444
216	CRIP2	cysteine-rich protein 2	1.32923
217	ARHGEF18	Rho/Rac guanine nucleotide exchange factor 18	1.32742
218	CEBPE	CCAAT/enhancer binding protein epsilon	1.32704
219	ETS2	v-ets avian erythroblastosis virus E26 oncogene homolog 2	1.31809
220	SIRPA	signal-regulatory protein alpha	1.3081
221	IFNGR1	interferon gamma receptor 1	1.30326
222	APBA3	amyloid beta (A4) precursor protein-binding, family A, member 3	1.29918
223	CREB3L1	cAMP responsive element binding protein 3-like 1	1.29846
224	WASF2	WAS protein family member 2	1.29785
225	KRT16	keratin 16, type I	1.29531
226	ANO6	anoctamin 6	1.29504
227	FPR1	formyl peptide receptor 1	1.2919
228	GBA	glucosidase, beta, acid	1.28636
229	NEURL1	neuralized E3 ubiquitin protein ligase 1	1.28481
230	EFNB1	ephrin-B1	1.28338

Number	Symbol	Entrez Gene Name	Fold Change
231	REPS2	RALBP1 associated Eps domain containing 2	1.28076
232	CAV1	caveolin 1	1.27821
233	FHOD1	formin homology 2 domain containing 1	1.2777
234	TBXAS1	thromboxane A synthase 1	1.27669
235	ID3	inhibitor of DNA binding 3, dominant negative helix-loop-helix protein	1.27432
236	KLK7	kallikrein related peptidase 7	1.27282
237	CTSB	cathepsin B	1.2722
238	E2F2	E2F transcription factor 2	1.26991
239	ATF2	activating transcription factor 2	1.26929
240	ANG	angiogenin, ribonuclease, RNase A family, 5	1.26295
241	FOXQ1	forkhead box Q1	1.26212
242	IGFBP3	insulin like growth factor binding protein 3	1.24814
243	KLF5	Kruppel-like factor 5 (intestinal)	1.24315
244	PEX11B	peroxisomal biogenesis factor 11 beta	1.24302
245	CTBP2	C-terminal binding protein 2	1.23906
246	GADD45A	growth arrest and DNA damage inducible alpha	1.23381
247	UNK	unkempt family zinc finger	1.22682
248	EPHB2	EPH receptor B2	1.22406
249	SEPT11	septin 11	1.21872
250	FLCN	folliculin	1.21512
251	LIMK2	LIM domain kinase 2	1.2114
252	ALOX5	arachidonate 5-lipoxygenase	1.21048
253	STARD13	StAR related lipid transfer domain containing 13	1.20956
254	KIF1C	kinesin family member 1C	1.20914
255	CEBPB	CCAAT/enhancer binding protein beta	1.20899
256	CFB	complement factor B	1.20881
257	PRKCZ	protein kinase C, zeta	1.20575
258	PML	promyelocytic leukemia	1.20095
259	WASF1	WAS protein family member 1	1.19908
260	MYO1E	myosin IE	1.19684
261	PPARA	peroxisome proliferator-activated receptor alpha	1.1953
262	MFI2	antigen p97 (melanoma associated) identified by monoclonal antibodies 133.2 and 96.5	1.19307
263	THRA	thyroid hormone receptor, alpha	1.19212
264	PLCG2	phospholipase C gamma 2	1.19
265	NOL3	nucleolar protein 3	1.18725
266	DCTN2	dynactin subunit 2	1.18711
267	SWAP70	SWAP switching B-cell complex 70kDa subunit	1.18608
268	TYRO3	TYRO3 protein tyrosine kinase	1.18563
269	OGG1	8-oxoguanine DNA glycosylase	1.18292

Number	Symbol	Entrez Gene Name	Fold Change
270	DOK1	docking protein 1	1.17558
271	LIMS2	LIM-type zinc finger domains 2	1.16949
272	GRHL2	grainyhead like transcription factor 2	1.16062
273	CDC42BPB	CDC42 binding protein kinase beta	1.16052
274	CDK5RAP3	CDK5 regulatory subunit associated protein 3	1.15733
275	ROBO4	roundabout guidance receptor 4	1.15231
276	MAPK7	mitogen-activated protein kinase 7	1.14122
277	NISCH	nischarin	1.1397
278	TXN	thioredoxin	1.13966
279	BATF3	basic leucine zipper transcription factor, ATF-like 3	1.1359
280	SPSB1	splA/ryanodine receptor domain and SOCS box containing 1	1.13579
281	RRAS	related RAS viral (r-ras) oncogene homolog	1.10437
282	LPAR4	lysophosphatidic acid receptor 4	1.0704
283	LILRB1	leukocyte immunoglobulin like receptor B1	1.06714
284	GPR18	G protein-coupled receptor 18	1.06277
285	SELP	selectin P	1.06242
286	SH2D3C	SH2 domain containing 3C	1.06103
287	IL16	interleukin 16	1.05912
288	ESR1	estrogen receptor 1	1.05874
289	PLXNC1	plexin C1	1.05869
290	BCL11B	B-cell CLL/lymphoma 11B	1.05823
291	CYP19A1	cytochrome P450 family 19 subfamily A member 1	1.05594
292	CCR8	chemokine (C-C motif) receptor 8	1.05587
293	EPB41L4B	erythrocyte membrane protein band 4.1 like 4B	1.05141
294	RARRES2	retinoic acid receptor responder (tazarotene induced) 2	1.04311

Down regulated genes

Number	Symbol	Entrez Gene Name	Fold Change
1	PHLDA1	pleckstrin homology-like domain, family A, member 1	−8.46535
2	TNFRSF11B	tumor necrosis factor receptor superfamily member 11b	−7.88483
3	PDE4B	phosphodiesterase 4B	−5.22171
4	IL6	interleukin 6	−4.46666
5	FGF5	fibroblast growth factor 5	−4.31595
6	CD36	CD36 molecule	−3.92846
7	IL1B	interleukin 1 beta	−3.74371
8	EREG	epiregulin	−3.51023
9	CCL2	chemokine (C-C motif) ligand 2	−3.41548
10	RUNX2	runt-related transcription factor 2	−2.95184
11	IGFBP5	insulin like growth factor binding protein 5	−2.92668

Number	Symbol	Entrez Gene Name	Fold Change
12	CXCL8	chemokine (C-X-C motif) ligand 8	−2.91859
13	CYP26A1	cytochrome P450 family 26 subfamily A member 1	−2.91556
14	PLAU	plasminogen activator, urokinase	−2.90533
15	IL24	interleukin 24	−2.88468
16	ST3GAL5	ST3 beta-galactoside alpha-2,3-sialyltransferase 5	−2.88077
17	SEMA3A	semaphorin 3A	−2.87725
18	TNFSF15	tumor necrosis factor superfamily member 15	−2.81580
19	FGFR1	fibroblast growth factor receptor 1	−2.76805
20	DIO2	deiodinase, iodothyronine, type II	−2.73236
21	TXK	TXK tyrosine kinase	−2.62840
22	SEMA3D	semaphorin 3D	−2.58360
23	FGFBP1	fibroblast growth factor binding protein 1	−2.51183
24	KCNA3	potassium channel, voltage gated shaker related subfamily A, member 3	−2.50982
25	FAT3	FAT atypical cadherin 3	−2.46791
26	CCRL2	chemokine (C-C motif) receptor-like 2	−2.45201
27	NPPB	natriuretic peptide B	−2.41923
28	ETV1	ets variant 1	−2.41900
29	LIF	leukemia inhibitory factor	−2.41840
30	CD28	CD28 molecule	−2.40401
31	EHF	ets homologous factor	−2.39617
32	SERPINB3	serpin peptidase inhibitor, clade B (ovalbumin), member 3	−2.37556
33	SEMA3E	semaphorin 3E	−2.35253
34	CSF2	colony stimulating factor 2	−2.34563
35	ST8SIA4	ST8 alpha-N-acetyl-neuraminide alpha-2,8-sialyltransferase 4	−2.32584
36	CEMIP	cell migration inducing protein, hyaluronan binding	−2.29345
37	FOSL1	FOS like antigen 1	−2.28415
38	TFPI2	tissue factor pathway inhibitor 2	−2.26858
39	BDNF	brain-derived neurotrophic factor	−2.24540
40	NR0B1	nuclear receptor subfamily 0 group B member 1	−2.23654
41	OPRM1	opioid receptor, mu 1	−2.23159
42	CCL3	chemokine (C-C motif) ligand 3	−2.22620
43	CYP1B1	cytochrome P450 family 1 subfamily B member 1	−2.20031
44	SCRN3	secernin 3	−2.13833
45	CSH1/CSH2	chorionic somatomammotropin hormone 1	−2.12536
46	SPRY4	sprouty RTK signaling antagonist 4	−2.12339
47	RGS4	regulator of G-protein signaling 4	−2.08806
48	NR2F1	nuclear receptor subfamily 2 group F member 1	−2.08334
49	IL23A	interleukin 23 subunit alpha	−2.08326
50	IFIT2	interferon induced protein with tetratricopeptide repeats 2	−2.07608

Number	Symbol	Entrez Gene Name	Fold Change
51	FOXA1	forkhead box A1	−2.06692
52	F3	coagulation factor III, tissue factor	−2.05004
53	ITGA2	integrin subunit alpha 2	−2.04652
54	CCDC40	coiled-coil domain containing 40	−2.04553
55	ZBTB18	zinc finger and BTB domain containing 18	−2.03725
56	GDNF	glial cell derived neurotrophic factor	−2.02472
57	CLDN11	claudin 11	−2.02083
58	IER3	immediate early response 3	−1.97907
59	NOG	noggin	−1.97215
60	BDKRB2	bradykinin receptor B2	−1.96909
61	CLDN1	claudin 1	−1.95484
62	GREM1	gremlin 1, DAN family BMP antagonist	−1.95480
63	CCL3L3	chemokine (C-C motif) ligand 3-like 3	−1.94494
64	ADAM19	ADAM metallopeptidase domain 19	−1.93804
65	ETV5	ets variant 5	−1.93529
66	STC1	stanniocalcin 1	−1.92768
67	CDH11	cadherin 11	−1.92589
68	CXCL1	chemokine (C-X-C motif) ligand 1 (melanoma growth stimulating activity, alpha)	−1.92384
69	CADM1	cell adhesion molecule 1	−1.92359
70	TNFRSF21	tumor necrosis factor receptor superfamily member 21	−1.91959
71	E2F5	E2F transcription factor 5, p130-binding	−1.91884
72	CD44	CD44 molecule (Indian blood group)	−1.91830
73	ADAMTS1	ADAM metallopeptidase with thrombospondin type 1 motif 1	−1.89520
74	SMAD3	SMAD family member 3	−1.86856
75	ADAM8	ADAM metallopeptidase domain 8	−1.86707
76	HBEGF	heparin-binding EGF-like growth factor	−1.85743
77	SOX9	SRY-box 9	−1.84049
78	NOV	nephroblastoma overexpressed	−1.83286
79	IRF8	interferon regulatory factor 8	−1.83215
80	GDF15	growth differentiation factor 15	−1.82966
81	HAVCR2	hepatitis A virus cellular receptor 2	−1.82840
82	LIPE	lipase, hormone-sensitive	−1.82349
83	SHC4	SHC (Src homology 2 domain containing) family member 4	−1.82181
84	ITGB8	integrin subunit beta 8	−1.81877
85	PRKCE	protein kinase C, epsilon	−1.81237
86	PTHLH	parathyroid hormone-like hormone	−1.79945
87	SPRY2	sprouty RTK signaling antagonist 2	−1.77757
88	PHLDA2	pleckstrin homology-like domain, family A, member 2	−1.76688
89	F2RL1	coagulation factor II (thrombin) receptor-like 1	−1.75500

Number	Symbol	Entrez Gene Name	Fold Change
90	HDAC9	histone deacetylase 9	−1.75136
91	CAMK2D	calcium/calmodulin-dependent protein kinase II delta	−1.74928
92	VEGFA	vascular endothelial growth factor A	−1.74782
93	IL21R	interleukin 21 receptor	−1.74709
94	MAP2K6	mitogen-activated protein kinase kinase 6	−1.74136
95	GPER1	G protein-coupled estrogen receptor 1	−1.73288
96	ADRA2A	adrenoceptor alpha 2A	−1.72940
97	CCND1	cyclin D1	−1.72596
98	CDCP1	CUB domain containing protein 1	−1.72023
99	CD274	CD274 molecule	−1.70099
100	WNT7B	wingless-type MMTV integration site family member 7B	−1.69513
101	MMP13	matrix metallopeptidase 13	−1.69399
102	WNT7A	wingless-type MMTV integration site family member 7A	−1.69365
103	SOX7	SRY-box 7	−1.68947
104	AQP3	aquaporin 3 (Gill blood group)	−1.68904
105	NGF	nerve growth factor (beta polypeptide)	−1.68514
106	VEGFC	vascular endothelial growth factor C	−1.67461
107	CFTR	cystic fibrosis transmembrane conductance regulator	−1.67311
108	CEACAM1	carcinoembryonic antigen related cell adhesion molecule 1	−1.67013
109	BCL3	B-cell CLL/lymphoma 3	−1.66934
110	EGF	epidermal growth factor	−1.66451
111	NUAK1	NUAK family, SNF1-like kinase, 1	−1.66163
112	MAP2K3	mitogen-activated protein kinase kinase 3	−1.65913
113	NUAK2	NUAK family, SNF1-like kinase, 2	−1.65090
114	PTX3	pentraxin 3	−1.65079
115	IL11	interleukin 11	−1.64764
116	TFAP2A	transcription factor AP-2 alpha (activating enhancer binding protein 2 alpha)	−1.64024
117	DUSP6	dual specificity phosphatase 6	−1.63858
118	EPAS1	endothelial PAS domain protein 1	−1.63589
119	DNMBP	dynamin binding protein	−1.62689
120	PLAUR	plasminogen activator, urokinase receptor	−1.62192
121	SLIT2	slit guidance ligand 2	−1.61888
122	AFAP1	actin filament associated protein 1	−1.61378
123	TM4SF1	transmembrane 4 L six family member 1	−1.60547
124	DLC1	DLC1 Rho GTPase activating protein	−1.60302
125	DLX2	distal-less homeobox 2	−1.59963
126	IL15RA	interleukin 15 receptor subunit alpha	−1.59691
127	DUSP4	dual specificity phosphatase 4	−1.59289
128	RASGRP1	RAS guanyl releasing protein 1 (calcium and DAG-regulated)	−1.58550

Number	Symbol	Entrez Gene Name	Fold Change
129	LTB	lymphotoxin beta	−1.58178
130	CLDN4	claudin 4	−1.57162
131	NR2F2	nuclear receptor subfamily 2 group F member 2	−1.56903
132	OSMR	oncostatin M receptor	−1.56874
133	LRP8	LDL receptor related protein 8	−1.56623
134	STX6	syntaxin 6	−1.56481
135	ST6GALNAC 5	ST6 (alpha-N-acetyl-neuraminyl-2,3-beta-galactosyl-1,3)-N-acetylgalactosaminide alpha-2,6-sialyltransferase 5	−1.56360
136	ABL2	ABL proto-oncogene 2, non-receptor tyrosine kinase	−1.56352
137	TCF4	transcription factor 4	−1.55623
138	MYO10	myosin X	−1.55431
139	PTAFR	platelet-activating factor receptor	−1.55164
140	SASH1	SAM and SH3 domain containing 1	−1.54902
141	NRG1	neuregulin 1	−1.54870
142	SFRP4	secreted frizzled-related protein 4	−1.54760
143	OLR1	oxidized low density lipoprotein (lectin-like) receptor 1	−1.54270
144	MMP1	matrix metallopeptidase 1	−1.54030
145	LYN	LYN proto-oncogene, Src family tyrosine kinase	−1.53885
146	CLDN3	claudin 3	−1.53743
147	SH3KBP1	SH3-domain kinase binding protein 1	−1.53570
148	EGLN3	egl-9 family hypoxia-inducible factor 3	−1.52322
149	PIK3CD	phosphatidylinositol-4,5-bisphosphate 3-kinase catalytic subunit delta	−1.51461
150	BACH2	BTB and CNC homology 1, basic leucine zipper transcription factor 2	−1.51327
151	FST	follistatin	−1.50979
152	SOCS3	suppressor of cytokine signaling 3	−1.50825
153	ADORA2B	adenosine A2b receptor	−1.50713
154	ETV6	ets variant 6	−1.50633
155	S100A7A	S100 calcium binding protein A7A	−1.50499
156	AMOTL1	angiomotin like 1	−1.49759
157	TMSB10/TM SB4X	thymosin beta 10	−1.49466
158	P2RY6	pyrimidinergic receptor P2Y, G-protein coupled, 6	−1.49425
159	RARRES1	retinoic acid receptor responder (tazarotene induced) 1	−1.49203
160	CXADR	coxsackie virus and adenovirus receptor	−1.49154
161	MMP2	matrix metallopeptidase 2	−1.48914
162	CCK	cholecystokinin	−1.48872
163	ODC1	ornithine decarboxylase 1	−1.48278
164	LDLR	low density lipoprotein receptor	−1.48242
165	SLC12A2	solute carrier family 12 (sodium/potassium/chloride transporter), member 2	−1.48129

Number	Symbol	Entrez Gene Name	Fold Change
166	SPNS2	spinster homolog 2 (Drosophila)	−1.47624
167	EPHB3	EPH receptor B3	−1.47347
168	HSP90AA1	heat shock protein 90kDa alpha family class A member 1	−1.47258
169	BDKRB1	bradykinin receptor B1	−1.46892
170	ITGA6	integrin subunit alpha 6	−1.46736
171	CMTM8	CKLF-like MARVEL transmembrane domain containing 8	−1.46426
172	C5AR1	complement component 5a receptor 1	−1.46246
173	KRAS	Kirsten rat sarcoma viral oncogene homolog	−1.45816
174	HTR7	5-hydroxytryptamine (serotonin) receptor 7, adenylate cyclase-coupled	−1.45507
175	CIITA	class II, major histocompatibility complex, transactivator	−1.45446
176	BHLHE41	basic helix-loop-helix family member e41	−1.45152
177	PTK2	protein tyrosine kinase 2	−1.44795
178	FAM60A	family with sequence similarity 60 member A	−1.44001
179	ID4	inhibitor of DNA binding 4, dominant negative helix-loop-helix protein	−1.43998
180	TCF7L2	transcription factor 7-like 2 (T-cell specific, HMG-box)	−1.43844
181	MESP1	mesoderm posterior bHLH transcription factor 1	−1.43834
182	TGFA	transforming growth factor alpha	−1.4379
183	CNN1	calponin 1, basic, smooth muscle	−1.4304
184	TFPI	tissue factor pathway inhibitor	−1.42959
185	ETV4	ets variant 4	−1.42898
186	HMGA2	high mobility group AT-hook 2	−1.42812
187	PELI1	pellino E3 ubiquitin protein ligase 1	−1.42779
188	LCP2	lymphocyte cytosolic protein 2	−1.42448
189	CTNNA2	catenin alpha 2	−1.42091
190	TYR	tyrosinase	−1.42076
191	TPM1	tropomyosin 1 (alpha)	−1.42072
192	SULT2B1	sulfotransferase family 2B member 1	−1.42007
193	ADAM12	ADAM metallopeptidase domain 12	−1.42003
194	SELL	selectin L	−1.41915
195	HAS3	hyaluronan synthase 3	−1.41793
196	RIPK2	receptor interacting serine/threonine kinase 2	−1.41689
197	SLC2A1	solute carrier family 2 (facilitated glucose transporter), member 1	−1.41412
198	AQP1	aquaporin 1 (Colton blood group)	−1.4135
199	CATSPERD	catsper channel auxiliary subunit delta	−1.41101
200	ETS1	v-ets avian erythroblastosis virus E26 oncogene homolog 1	−1.411
201	SCN9A	sodium channel, voltage gated, type IX alpha subunit	−1.4108
202	SMAD7	SMAD family member 7	−1.40998
203	ICAM1	intercellular adhesion molecule 1	−1.40688
204	HGF	hepatocyte growth factor (hepapoietin A; scatter factor)	−1.40635

Number	Symbol	Entrez Gene Name	Fold Change
205	IGF1R	insulin like growth factor 1 receptor	−1.40444
206	SYNM	synemin	−1.40255
207	PODXL	podocalyxin-like	−1.40063
208	CLEC7A	C-type lectin domain family 7 member A	−1.40008
209	STK35	serine/threonine kinase 35	−1.3991
210	ADORA3	adenosine A3 receptor	−1.39827
211	NR1D1	nuclear receptor subfamily 1 group D member 1	−1.39569
212	ZDHHC20	zinc finger, DHHC-type containing 20	−1.39423
213	FOXP1	forkhead box P1	−1.39132
214	CAPN12	calpain 12	−1.39041
215	ATP1A4	ATPase, Na+/K+ transporting, alpha 4 polypeptide	−1.38932
216	CXCL2	chemokine (C-X-C motif) ligand 2	−1.38857
217	JAG1	jagged 1	−1.388
218	RUNX1	runt-related transcription factor 1	−1.38576
219	RASSF5	Ras association (RalGDS/AF-6) domain family member 5	−1.38344
220	MYH11	myosin, heavy chain 11, smooth muscle	−1.37585
221	PPIF	peptidylprolyl isomerase F	−1.37223
222	AJAP1	adherens junctions associated protein 1	−1.37108
223	IGHG1	immunoglobulin heavy constant gamma 1 (G1m marker)	−1.37108
224	SNAI1	snail family zinc finger 1	−1.36983
225	EIF4E	eukaryotic translation initiation factor 4E	−1.36964
226	RASGRF1	Ras protein specific guanine nucleotide releasing factor 1	−1.36863
227	PTPRK	protein tyrosine phosphatase, receptor type K	−1.36543
228	CDC42EP1	CDC42 effector protein 1	−1.36535
229	GCNT2	glucosaminyl (N-acetyl) transferase 2, I-branching enzyme (I blood group)	−1.36516
230	DEFB103A/DEFB103B	defensin beta 103B	−1.36313
231	VDR	vitamin D (1,25- dihydroxyvitamin D3) receptor	−1.36297
232	PARD6B	par-6 family cell polarity regulator beta	−1.36193
233	IER2	immediate early response 2	−1.36131
234	DLL1	delta-like 1 (Drosophila)	−1.36055
235	PTPRR	protein tyrosine phosphatase, receptor type R	−1.35893
236	CATSPER1	cation channel, sperm associated 1	−1.3582
237	WNT4	wingless-type MMTV integration site family member 4	−1.34903
238	PTP4A1	protein tyrosine phosphatase type IVA, member 1	−1.34726
239	TNFRSF10A	tumor necrosis factor receptor superfamily member 10a	−1.34601
240	EPHB1	EPH receptor B1	−1.34462
241	TNFRSF12A	tumor necrosis factor receptor superfamily member 12A	−1.34406
242	GEMIN5	gem nuclear organelle associated protein 5	−1.34324

Number	Symbol	Entrez Gene Name	Fold Change
243	LMO4	LIM domain only 4	−1.34176
244	FUT8	fucosyltransferase 8 (alpha (1,6) fucosyltransferase)	−1.3409
245	MYF5	myogenic factor 5	−1.33933
246	NAA15	N(alpha)-acetyltransferase 15, NatA auxiliary subunit	−1.33862
247	DNAJB6	DnaJ heat shock protein family (Hsp40) member B6	−1.33628
248	AGTR2	angiotensin II receptor type 2	−1.33574
249	MITF	microphthalmia-associated transcription factor	−1.33566
250	CHL1	cell adhesion molecule L1-like	−1.33449
251	WISP2	WNT1 inducible signaling pathway protein 2	−1.33436
252	TLR3	toll-like receptor 3	−1.33216
253	PRSS27	protease, serine 27	−1.32726
254	FUT3	fucosyltransferase 3 (Lewis blood group)	−1.32708
255	GLRX	glutaredoxin	−1.3242
256	TGFBI	transforming growth factor beta induced	−1.32276
257	KNG1	kininogen 1	−1.32215
258	ONECUT2	one cut homeobox 2	−1.32092
259	RBFOX2	RNA binding protein, fox-1 homolog (C. elegans) 2	−1.3207
260	TSHR	thyroid stimulating hormone receptor	−1.32046
261	HSP90AB1	heat shock protein 90kDa alpha family class B member 1	−1.31987
262	GAD1	glutamate decarboxylase 1	−1.31719
263	SPAG9	sperm associated antigen 9	−1.31697
264	FGF2	fibroblast growth factor 2 (basic)	−1.31569
265	SOCS4	suppressor of cytokine signaling 4	−1.31507
266	IL17RB	interleukin 17 receptor B	−1.3143
267	PIK3CG	phosphatidylinositol-4,5-bisphosphate 3-kinase catalytic subunit gamma	−1.31388
268	MNX1	motor neuron and pancreas homeobox 1	−1.31094
269	ASPH	aspartate beta-hydroxylase	−1.31058
270	PDGFB	platelet derived growth factor subunit B	−1.30629
271	SYNJ2BP	synaptojanin 2 binding protein	−1.30419
272	VAV1	vav guanine nucleotide exchange factor 1	−1.30245
273	PLPP3	phospholipid phosphatase 3	−1.30085
274	RELB	v-rel avian reticuloendotheliosis viral oncogene homolog B	−1.29866
275	YWHAQ	tyrosine 3-monooxygenase/tryptophan 5-monooxygenase activation protein, theta	−1.29533
276	NDST1	N-deacetylase/N-sulfotransferase (heparan glucosaminyl) 1	−1.28877
277	DYX1C1	dyslexia susceptibility 1 candidate 1	−1.28795
278	CLEC5A	C-type lectin domain family 5 member A	−1.28692
279	POMK	protein-O-mannose kinase	−1.28647
280	ZFAND5	zinc finger, AN1-type domain 5	−1.28575
281	SMN1/SMN2	survival of motor neuron 1, telomeric	−1.28521

Number	Symbol	Entrez Gene Name	Fold Change
282	EFNA1	ephrin-A1	−1.28027
283	VTCN1	V-set domain containing T cell activation inhibitor 1	−1.27926
284	AMD1	adenosylmethionine decarboxylase 1	−1.27848
285	RND3	Rho family GTPase 3	−1.27788
286	DCBLD2	discoidin, CUB and LCCL domain containing 2	−1.27761
287	GJA1	gap junction protein alpha 1	−1.27588
288	HOXA2	homeobox A2	−1.27472
289	TWIST2	twist family bHLH transcription factor 2	−1.273
290	ADGRG1	adhesion G protein-coupled receptor G1	−1.26945
291	PIK3C2B	phosphatidylinositol-4-phosphate 3-kinase catalytic subunit type 2 beta	−1.26945
292	NAMPT	nicotinamide phosphoribosyltransferase	−1.26749
293	PRMT6	protein arginine methyltransferase 6	−1.26295
294	TRAF3	TNF receptor associated factor 3	−1.26024
295	EZR	ezrin	−1.25889
296	PPP1R15A	protein phosphatase 1 regulatory subunit 15A	−1.25828
297	DRAM1	DNA damage regulated autophagy modulator 1	−1.25703
298	SNCA	synuclein alpha	−1.25233
299	OCLN	occludin	−1.25226
300	KCNK5	potassium channel, two pore domain subfamily K, member 5	−1.25156
301	PRLR	prolactin receptor	−1.2486
302	BCAR1	breast cancer anti-estrogen resistance 1	−1.24785
303	NFAT5	nuclear factor of activated T-cells 5, tonicity-responsive	−1.24658
304	RAC2	ras-related C3 botulinum toxin substrate 2 (rho family, small GTP binding protein Rac2)	−1.24535
305	MALT1	MALT1 paracaspase	−1.24468
306	HHEX	hematopoietically expressed homeobox	−1.24069
307	DNAJA1	DnaJ heat shock protein family (Hsp40) member A1	−1.23969
308	NET1	neuroepithelial cell transforming 1	−1.23934
309	TCAF1	TRPM8 channel-associated factor 1	−1.239
310	ARHGAP19	Rho GTPase activating protein 19	−1.23845
311	ZNF652	zinc finger protein 652	−1.23649
312	CCL26	chemokine (C-C motif) ligand 26	−1.23552
313	MIEN1	migration and invasion enhancer 1	−1.2349
314	SMG1	SMG1 phosphatidylinositol 3-kinase-related kinase	−1.23249
315	MYO5B	myosin VB	−1.23164
316	RAG1	recombination activating gene 1	−1.2303
317	CGB3 (includes others)	chorionic gonadotropin beta subunit 3	−1.22918
318	RALGAPA2	Ral GTPase activating protein, alpha subunit 2 (catalytic)	−1.22615

Number	Symbol	Entrez Gene Name	Fold Change
319	B4GALT5	UDP-Gal:betaGlcNAc beta 1,4- galactosyltransferase, polypeptide 5	−1.22529
320	GSK3B	glycogen synthase kinase 3 beta	−1.22451
321	CDK6	cyclin-dependent kinase 6	−1.22402
322	CTNNAL1	catenin alpha-like 1	−1.22048
323	CD58	CD58 molecule	−1.21835
324	CYR61	cysteine rich angiogenic inducer 61	−1.21306
325	ZNF24	zinc finger protein 24	−1.21218
326	DGKE	diacylglycerol kinase epsilon	−1.21008
327	PTEN	phosphatase and tensin homolog	−1.20912
328	WWC1	WW and C2 domain containing 1	−1.20909
329	SFRP1	secreted frizzled-related protein 1	−1.20491
330	ABHD6	abhydrolase domain containing 6	−1.20477
331	NEU1	neuraminidase 1 (lysosomal sialidase)	−1.19821
332	UBE2I	ubiquitin conjugating enzyme E2I	−1.19721
333	EBI3	Epstein-Barr virus induced 3	−1.19684
334	ZEB2	zinc finger E-box binding homeobox 2	−1.19545
335	MMP16	matrix metallopeptidase 16	−1.19347
336	CD93	CD93 molecule	−1.19321
337	ANXA1	annexin A1	−1.19311
338	P4HA2	prolyl 4-hydroxylase, alpha polypeptide II	−1.19140
339	ATP6V1C1	ATPase, H+ transporting, lysosomal 42kDa, V1 subunit C1	−1.19127
340	BBS4	Bardet-Biedl syndrome 4	−1.19104
341	SRPX2	sushi-repeat containing protein, X-linked 2	−1.19022
342	CXCR6	chemokine (C-X-C motif) receptor 6	−1.19013
343	TAC1	tachykinin precursor 1	−1.18419
344	FAM188A	family with sequence similarity 188 member A	−1.18353
345	NFKB1	nuclear factor of kappa light polypeptide gene enhancer in B-cells 1	−1.18152
346	BAG1	BCL2 associated athanogene 1	−1.17465
347	EHD1	EH domain containing 1	−1.17454
348	LIMA1	LIM domain and actin binding 1	−1.17448
349	MOV10L1	Mov10 RISC complex RNA helicase like 1	−1.17430
350	ADGRE5	adhesion G protein-coupled receptor E5	−1.17397
351	COPB2	coatomer protein complex subunit beta 2 (beta prime)	−1.17383
352	NR3C1	nuclear receptor subfamily 3 group C member 1	−1.16742
353	CLEC11A	C-type lectin domain family 11 member A	−1.16735
354	PI4KB	phosphatidylinositol 4-kinase, catalytic, beta	−1.16700
355	ACP1	acid phosphatase 1, soluble	−1.16609
356	C1QBP	complement component 1, q subcomponent binding protein	−1.16280

Number	Symbol	Entrez Gene Name	Fold Change
357	PTTG1	pituitary tumor-transforming 1	−1.16060
358	PRRX1	paired related homeobox 1	−1.15954
359	SMAD1	SMAD family member 1	−1.15936
360	ADM	adrenomedullin	−1.15071
361	NDRG2	NDRG family member 2	−1.14999
362	REST	RE1-silencing transcription factor	−1.14731
363	NINJ1	ninjurin 1	−1.14059
364	CDKN3	cyclin-dependent kinase inhibitor 3	−1.13962
365	CIB1	calcium and integrin binding 1	−1.13924
366	HSPD1	heat shock protein family D (Hsp60) member 1	−1.13652
367	MS4A4A	membrane-spanning 4-domains subfamily A member 4A	−1.13410
368	LGALS8	lectin, galactoside-binding, soluble, 8	−1.12928
369	VPS28	vacuolar protein sorting 28 homolog (S. cerevisiae)	−1.12857
370	PODN	podocan	−1.12805
371	IL25	interleukin 25	−1.12250
372	TMPRSS4	transmembrane protease, serine 4	−1.12108
373	GRB2	growth factor receptor bound protein 2	−1.11159
374	PEX13	peroxisomal biogenesis factor 13	−1.11146
375	PLCL1	phospholipase C like 1	−1.10743
376	CD48	CD48 molecule	−1.10057
377	ASTN1	astrotactin 1	−1.09980
378	IQUB	IQ motif and ubiquitin domain containing	−1.09258
379	RNASE2	ribonuclease, RNase A family, 2 (liver, eosinophil-derived neurotoxin)	−1.08789
380	AQP4	aquaporin 4	−1.08643
381	PRKCB	protein kinase C, beta	−1.08474
382	SATB2	SATB homeobox 2	−1.07941
383	GRIA3	glutamate receptor, ionotropic, AMPA 3	−1.06982
384	CCDC39	coiled-coil domain containing 39	−1.06883
385	PECAM1	platelet/endothelial cell adhesion molecule 1	−1.06057